Journal of Computational Physics 229 (2010) 4183–4207

Contents lists available at ScienceDirect

Journal of Computational Physics

journal homepage: www.elsevier.com/locate/jcp

The equilibrium limit of a constitutive model for two-phase granular mixtures and its numerical approximation

C. Varsakelis, M.V. Papalexandris *

Departément de Mécanique, Université catholique de Louvain, 1348 Louvain la Neuve, Belgium

ARTICLE INFO

Article history:
Received 21 September 2009
Received in revised form 4 February 2010
Accepted 5 February 2010
Available online 14 February 2010

Keywords:
Granular mixtures
Complex fluids
Overdetermined elliptic systems
Ladyzhenskaya's theorem
Successive-over-relaxation
Predictor–corrector methods

ABSTRACT

In this paper we analyze the equilibrium limit of the constitutive model for two-phase granular mixtures introduced in Papalexandris (2004) [13], and develop an algorithm for its numerical approximation. At, equilibrium, the constitutive model reduces to a strongly coupled, overdetermined system of quasilinear elliptic partial differential equations with respect to the pressure and the volume fraction of the solid granular phase. First we carry a perturbation analysis based on standard hydrostatic-type scaling arguments which reduces the complexity of the coupling of the equations. The perturbed system is then supplemented by an appropriate compatibility condition which arises from the properties of the gradient operator. Further, based on the Helmholtz decomposition and Ladyzhenskaya's decomposition theorem, we develop a projection-type, Successive-Over-Relaxation numerical method. This method is general enough and can be applied to a variety of continuum models of complex mixtures and mixtures with micro-structure. We also prove that this method is both stable and consistent hence, under standard assumptions, convergent. The paper concludes with the presentation of representative numerical results.

1. Introduction

Two-phase flows of granular mixtures are encountered in numerous industrial and technological applications (mining, pharmaceutical and process industries, power plants, propulsion, etc.) as well as in agriculture, geophysical processes, and elsewhere. Because of the wide applicability of these flows, many research efforts have been devoted to their modelling and simulation; see, for example, [1–8] and references therein. However, despite the long reference list and considerable progress in this field, our understanding of such flows is still not satisfactory. At present, a general theoretical framework for the description of granular flows does not exist. In fact, it has been observed that nearly 60% of the transport and storage capacity of granular materials is lost due to poorly developed theory [9]. Further, due to lack of efficient and robust algorithms, the numerical treatment of the flows of interest has been limited to very special cases.

Typically, the derivation of mathematical models of two-phase granular flows employs either an averaging or a mixture-theory approach. Both approaches have advantages and drawbacks associated with them. The averaging approach employs aspects from kinetic theories and is based on modifying the equations of motion of a single constituent to account for the presence of the other constituents and then averaging these equations over space and/or time, [10,11]. These averages can be set equal to ensemble averages if the system is ergodic. Its main advantage is that it is a "first principles" approach and, therefore, requires a few initial postulates. However, collisions between grains are often modelled, if at all,

* Corresponding author. Tel.: +32 10 47 88 83; fax: +32 10 45 26 92.
E-mail address: miltos@uclouvain.be (M.V. Papalexandris).

0021-9991/$ - see front matter © 2010 Elsevier Inc. All rights reserved.
doi:10.1016/j.jcp.2010.02.005

in a rudimentary way. Another drawback of this approach is that the averaging process relies on assumptions whose validity for the problem in hand is questionable. Examples include the ergodic hypothesis and the assumption that the number of grains is large enough to lie in the validity range of the law of large numbers.

On the other hand, mixture theories treat the system as a multi-component continuum and adopt a non-equilibrium thermodynamic formalism for the derivation of the balance equations for each phase. This is achieved by employing the constraints imposed by the entropy inequality law, which in turn enables the derivation of constitutive relations for the irreversible phenomena that take place, such as, viscosity, heat transfer, phase interactions, etc. This approach has the advantage that it provides a set of governing equations in a straightforward and elegant way. However, this approach has scale-related limitations stemming from the continuum hypothesis: the size of the grains has to be orders of magnitude smaller than the size of the flow domain. Further, all limitations and drawbacks of the thermodynamic formalism used for the derivation of the mathematical model carry over to the model itself. The interested reader is referred to [10,12] for self-contained presentations and descriptions of both approaches.

In [13], the second author derived a model for compressible two-phase flows of granular mixtures based on an extension of the theory of irreversible processes [14,15]. This model can be considered as a two-phase generalization of the Navier–Stokes–Fourier equations for simple fluids which, in addition, takes into account the fact that granular materials support shear at equilibrium. More specifically, the model introduces the volume fraction of each phase and its spatial gradient as independent thermodynamic variables. These variables are related to the micro-structure of the system and model forces that are developed at the grain level. The Gibbs equation for each phase is then generalized to include the contributions from these new variables, in the form of reversible work performed by the corresponding additional forces.

The volume fraction gradients, in particular, are introduced for the description of non-local effects whose macroscopic manifestation is the presence of shear in the equilibrium. These shear stresses are known to depend on the intergranular surface area and the interfacial surface. On the other hand, the volume fraction gradient is by definition a measure of the interfacial area density and is thus, a natural choice for the modelling of such stresses. As a matter of fact, the use of the spatial gradients for the description of non-local effects is an old idea, first introduced by Landau in his theory of phase transitions, [16].

In this paper we present and analyze an algorithm for the numerical approximation of the equilibrium behavior of two-phase granular mixtures, as predicted by the model in [13]. At equilibrium, this model reduces to a set of overdetermined, quasilinear elliptic equations in terms of the volume fraction and the pressure of the granular material. We note that the equilibrium equations admit spatially structured solutions for both the pressure and the volume fraction and, therefore, their study is far from trivial.

Based on standard hydrostatic-type scaling arguments we first perform a perturbation analysis for the system in hand. The perturbed system is then supplemented by an appropriate compatibility condition which arises from the cohomologies of the gradient operator. Subsequently, we design a projection-type, Successive-over-relaxation algorithm for the perturbed system based on the combination of the Helmholtz decomposition and Ladyzhenskaya's theorem for the construction of the orthogonal complement of the Lebesgue-square-integrable solenoidal vector fields.

The main objectives of our work are the following.

(i) To develop a numerical framework for accurately predicting the multi-dimensional structure of two-phase granular mixtures at equilibrium. To the best of our knowledge, such framework currently does not exist. This numerical framework can also serve as a tool for testing the validity of mathematical models based on mixture theories, such as the one proposed in [13]. In fact, the accurate prediction of the equilibrium distributions is a necessary, but not sufficient, condition for every model that aims to describe two-phase flows of granular mixtures.
(ii) To gain physical insight on the equilibrium distribution of immiscible mixtures and on the interplay between the various forces acting on them at equilibrium. Currently, multi-dimensional numerical results for equilibria of such mixtures are available only for very special cases.
(iii) To perform the first step toward the development of efficient numerical methods for flows of granular mixtures. In this respect it is particularly interesting to study the numerical approximation of the terms describing non-local effects and relaxation phenomena.

It is important to mention that the proposed numerical method is applicable to other models, different than the equilibrium limit of the model in [13]. It can be applied to a whole class of equations that describe equilibria of mixtures and complex fluids. This is because, as will be shown later, the non-classical terms in the momentum equation, such as those describing non-local effects, are treated numerically as source terms. Thus, despite the fact that the exact form of these non-classical terms can vary among different models, our method treats them in the same fashion.

This paper is organized as follows. In Section 2 we present the equilibrium equations and we develop the theoretical framework for the numerical method. In Section 3 the numerical algorithm is presented in detail. Section 4 is devoted to the stability and consistency analysis. In Section 5 we discuss possible approaches for cases not covered by the perturbation analysis. Finally, in Section 6, we present some representative results from the numerical experiments that we conducted in the course of our study. For the sake of completeness and self-containment, the full model of [13] is presented in the Appendix.

Throughout this paper we adopt the following, classical, notation.

- Ω stands for a Lipschitz, convex and bounded domain of $\mathbb{R}^n,\ n = 2, 3$.
- $L^2(\Omega), L^{2,2}(\Omega)$ stands for space of Lebesgue-square-integrable measurable functions-vector fields in Ω, with corresponding norm $\|\ \|_{L^2}$, and $\|\ \|_{L^{2,2}}$.
- $H^i(\Omega),\ i \in \mathbb{N}$ stands for the Sobolev space of $L^2(\Omega)$-functions whose weak derivatives up to order i belong in $L^2(\Omega)$, with norm $\|\ \|_{H^i}$.
- $C^i(\Omega)$ is the space of functions which have continuous derivatives up to degree i.
- $\mathcal{H}((0,T) : X(\Omega))$, where $X, \mathcal{H}$ are Banach spaces, stands for the Bochner space [17] of functions

  $f : \Omega \times (0,T) \to \mathbb{R}$,

  which satisfy the condition

  $\| \|f\|_{X(\Omega)}\|_{\mathcal{H}(0,T)} < \infty$.
- Given a function or a vector $u(x)$, $\|u\|_{\max}$ will denote the standard sup-norm *i.e.*

  $\|u\|_{\max} = \sup_{x\in\Omega} |u(x)|$.

  Moreover, given a matrix $A \in \mathbb{R}^{N\times M}$ $\|A\|_\infty$ will correspond to the norm defined by the relation

  $\|A\|_\infty = \max_{1\leqslant i\leqslant N} \sum_{j=1}^{M} |A_{ij}|$.
- **n** will denote the unit normal vector field in the boundary of the domain of our interest. Since the domain of our interest will be always assumed to be Lipschitz, we will not have existence problems for **n**.
- The "hat" symbol '^' over a variable will denote that the variable is in dimensional form. Variables without the "hat" symbol are understood to be in non-dimensional form.

Finally, we adopt the following index convention throughout this paper. The index "*s*" stands for the solid phase, *i.e.*, the granular material, while the index "*f*" stands for the fluid phase.

2. The equilibrium equations

Let us assume that we are given a saturated mixture of an isotropic granular material and a fluid, in the domain Ω. Furthermore, we assume absence of chemical reactions and phase changes.

The model derived in [13] introduces the volume fractions and their spatial gradients as independent intensive thermodynamic variables. The use of the volume fraction as a thermodynamic variable is standard in the framework of multi-component flows. Its usual interpretation as a concentration parameter is that "the mixture is assumed to consist of two coexisting continua". However, this interpretation is misleading and unsatisfactory from the physical point of view because it is obviously invalid at the mesoscopic (grain) level, as a consequence of the fact that granular materials do not exhibit a scale segregation. In fact, in many granular mixtures, even the naked eye can observe the phase separation and determine if a given point in space is occupied by one phase or the other. Thus, the usual averaging approaches for its definition fail, since the limit does not exist.

For this reason, in our point of view, it is more appropriate to interpret the volume fraction as the probability of finding one phase or the other in a given volume (measurable set) in space and at a given time. This interpretation naturally leads to the following formal definition of the volume fraction, proposed by Goodman and Cowin [1],

Definition 2.0.1. Let $\mu(x)$ stand for the natural Lebesgue measure in Ω with corresponding σ-algebra $\mathcal{S}$. Define the measure $\mu_s(x)$ as follows: for any Lebesgue measurable set $A \subset \Omega$,

$$\mu_s(A) = \frac{\int_A 1_s \mathrm{d}\mu(x)}{\mu(A)},$$

where 1_s is the indicator function for the solid phase. $\mu_s(x)$ is absolutely continuous with respect to $\mu(x)$ and, therefore, by the Radon–Nikodym theorem, $\exists \phi \in L^1(\Omega)$ such as

$$\mu_s(A) = \int_A \phi_s(x)\ \mathrm{d}\mu(x), \quad \forall A \in \mathcal{S}.$$

The normalized (probability) density function ϕ_s is defined as the volume fraction of the granular material.

Under the above definition of the volume fraction as a probability density function, the so-called "coexistence of the two phases" admits a probabilistic (or measure-theoretic) interpretation. This interpretation is both physically meaningful and consistent with the measure-theoretic framework of thermodynamics. Definition 2.0.1 describes a stationary probability

distribution. The evolution of the dynamical system, *i.e*, the system of PDEs, that governs the behavior of the flow of the granular mixture, corresponds to the one-parameter family of distributions $\{\phi_s(t)\}_{t=t_{in}}^{\infty}$, where t_{in} is the initial time of the flow. Then, $\{\phi_s(t)\}_{t=t_{in}}^{\infty}$ is the evolution of densities and it is generally given by a non-linear Markov operator. Therefore, the volume fraction is well-posed as a spatio-temporal distribution.

It is worth mentioning that the measure-theoretic interpretation of the volume fraction does not play a role in the development of the proposed numerical method. However, this interpretation of the volume fraction is important not only from the physical but also from the mathematical points of view. For example, the fact that an equation admits solutions that are Radon–Nikodym densities has implications in the derivation of existence and regularity results for these equations.

Finally, we assume throughout the paper that the volume fractions of the two phases ϕ_s, ϕ_f are uniformly bounded away from zero. This assumption is made because the passing to the single-phase equations is highly singular and beyond the scope of the present study.

At equilibrium, the temperatures of the two phases $\widehat{T}_s, \widehat{T}_f$ are equal and uniform, the velocities of the two phases are zero everywhere, and all the terms in the model that describe dissipative processes are zero. Under the assumption that the fluid phase behaves like a simple Newtonian fluid, the mathematical model in [13], see Appendix, at equilibrium reduces to

$$\widehat{\nabla}((\hat{p}_s - \hat{p}_f)\phi_s) = -\widehat{\nabla}\cdot(\widehat{\Gamma}_s\widehat{\nabla}\phi_s\otimes\widehat{\nabla}\phi_s) - \phi_s(\hat{\rho}_s - \hat{\rho}_f)\hat{\mathbf{g}}, \tag{1}$$

$$\widehat{\nabla}\hat{p}_f = -\hat{\rho}_f\hat{\mathbf{g}}, \tag{2}$$

$$\hat{p}_s - \hat{p}_f = \hat{\beta}_s - \widehat{\nabla}\cdot(\widehat{\Gamma}_s\widehat{\nabla}\phi_s), \tag{3}$$

where $\hat{p}_i, \hat{\rho}_i, \phi_i, i = s,f$, stand for the pressure, density, and volume fraction of the ith phase, respectively, and $\hat{\mathbf{g}}$ is the acceleration due to gravity.

Eqs. (1) and (2) result from the momentum equations for the solid and fluid phase, respectively, and express the balance of forces acting on each phase at equilibrium. Further, Eq. (3) is the equilibrium limit of the compaction equation, which is a rate equation for the solid volume fraction, see Appendix.

The system (1)–(3) is closed by the saturation condition,

$$\phi_s(x) + \phi_f(x) = 1 \quad \text{almost everywhere } \in \Omega, \tag{4}$$

and appropriate equations of state. For the sake of simplicity, we assume that the fluid phase obeys the perfect gas equation of state,

$$\hat{p}_f = R_f\hat{\rho}_f\widehat{T}_f, \tag{5}$$

where R_f is the gas constant. Additionally, the material of the granular phase is assumed to follow the stiffened gas equation of state,

$$\hat{p}_s + \widehat{P}_\infty = R_s\hat{\rho}_s\widehat{T}_s, \tag{6}$$

where $\widehat{P}_\infty$ stands for the "correction pressure" and R_s is the solid material's constant. As it will be shown later, the detailed expression of the equation of state for the constituents of the mixture does not play a role in the derivation of the numerical method.

Further, in the system (1)–(3), the variable $\hat{\beta}_s$ stands for the so-called configuration pressure [1] and represents the contact forces that are developed between granular grains. Also, the expression inside the divergence term in (1) that contains $\widehat{\Gamma}_s$ represents an additional stress tensor due to non-local effects associated with the micro-structure of the granular material. The presence of these additional stresses is a manifestation of the fact that granular materials can support shear at equilibrium. Henceforth, this stress tensor is referred to as the *residual stress tensor*,

$$\hat{\boldsymbol{\sigma}} = \widehat{\Gamma}_s\widehat{\nabla}\phi_s\otimes\widehat{\nabla}\phi_s. \tag{7}$$

The quantities $\hat{\beta}_s$ and $\widehat{\Gamma}_s$ are defined via the granular material's Helmholtz free energy $\hat{\psi}_s$ as follows,

$$\hat{\beta}_s = \hat{\rho}_s\phi_s\frac{\partial\hat{\psi}_s}{\partial\phi_s}, \quad \widehat{\Gamma}_s = 2\hat{\rho}_s\phi_s\frac{\partial\hat{\psi}_s}{\partial(\widehat{\nabla}\phi_s\cdot\widehat{\nabla}\phi_s)}. \tag{8}$$

This definition of $\hat{\beta}_s$ and $\widehat{\Gamma}_s$ suggests the following decomposition of $\hat{\psi}_s$,

$$\hat{\psi}_s = \hat{\psi}_s^p + \hat{\psi}_p^c, \tag{9}$$

where $\hat{\psi}_s^p$ is the free energy of the pure material that the grains consist of, and $\hat{\psi}_s^c$ is the remaining part. Therefore, $\hat{\psi}_s^p$ is independent of ϕ_s, whereas $\hat{\psi}_s^c$ is associated with compaction and rearrangement of interfacial area density.

As with all equations of state, the exact functional form of $\hat{\psi}_s^c$ is material dependent and has to be confirmed experimentally. However, and to the best of our knowledge, detailed experimental measurements of the compaction free energy in a variety of physical conditions currently do not exist in the literature. For this reason, researchers in the field have considered various *ad hoc* functional forms in the past. Nonetheless, every proposed expression for $\hat{\psi}_s^c$ must satisfy the convexity requirements for the stability of thermodynamic equilibria.

In our study we assume that $\hat{\psi}_s^c$ does not depend on the solid material's pressure and density; see also the discussion in [4]. Further, and by virtue of the fact that $\widehat{\Gamma}_s$ is the coefficient of the elliptic operator in Eq. (3), we require that $\hat{\psi}_s^c$ is such that (i) $\widehat{\Gamma}_s$ and $\hat{\beta}$ are bounded, and (ii) $\widehat{\Gamma}_s$ is strictly positive almost everywhere in Ω. If these requirements are satisfied, the ellipticity of the system is guaranteed, see Section 2.1.

In this article we choose $\hat{\psi}_s^c$ to be a simple convex function,

$$\hat{\psi}_s^c = \frac{1}{2}\left(\hat{k}_1\phi_s^2 + \hat{k}_2(\widehat{\nabla}\phi_s)^2\right), \tag{10}$$

where $\hat{k}_1, \hat{k}_2 \geqslant 0$ are constants related to the granular medium under study. It can be easily verified that, by virtue of the strict positivity of ϕ_s, this choice of $\hat{\psi}_s^c$ satisfies the above requirements. However, it is important to mention that all theoretical results and the numerical method presented in this article hold for all functional forms of $\hat{\psi}_s^c$ that satisfy the above requirements

Combining Eqs. (8) and (10) yields the following analytical expressions,

$$\hat{\beta}_s = \hat{k}_1\hat{\rho}_s\phi_s^2, \quad \widehat{\Gamma}_s = \hat{k}_2\hat{\rho}_s\phi_s. \tag{11}$$

Under this choice the convexity criteria of stability of thermodynamic equilibria, are obviously satisfied. Moreover, two interesting observations can be made. First, the symmetric residual stress tensor $\hat{\boldsymbol{\sigma}}$ has the analytical representation,

$$\hat{\boldsymbol{\sigma}} = \begin{pmatrix} \hat{\sigma}_{11} & \hat{\sigma}_{12} & \hat{\sigma}_{13} \\ \hat{\sigma}_{12} & \hat{\sigma}_{22} & \hat{\sigma}_{23} \\ \hat{\sigma}_{31} & \hat{\sigma}_{32} & \hat{\sigma}_{33} \end{pmatrix} = \hat{k}_2\hat{\rho}_s\phi_s \begin{pmatrix} \frac{\partial\phi_s}{\partial\hat{x}}\frac{\partial\phi_s}{\partial\hat{x}} & \frac{\partial\phi_s}{\partial\hat{x}}\frac{\partial\phi_s}{\partial\hat{y}} & \frac{\partial\phi_s}{\partial\hat{x}}\frac{\partial\phi_s}{\partial\hat{z}} \\ \frac{\partial\phi_s}{\partial\hat{x}}\frac{\partial\phi_s}{\partial\hat{y}} & \frac{\partial\phi_s}{\partial\hat{y}}\frac{\partial\phi_s}{\partial\hat{y}} & \frac{\partial\phi_s}{\partial\hat{y}}\frac{\partial\phi_s}{\partial\hat{z}} \\ \frac{\partial\phi_s}{\partial\hat{x}}\frac{\partial\phi_s}{\partial\hat{z}} & \frac{\partial\phi_s}{\partial\hat{y}}\frac{\partial\phi_s}{\partial\hat{z}} & \frac{\partial\phi_s}{\partial\hat{z}}\frac{\partial\phi_s}{\partial\hat{z}} \end{pmatrix}.$$

Second, the overall Helmholtz free energy of the system, *i.e.*, the extensive version of $\hat{\psi}_s^c$,

$$\widehat{\Psi}_s^c = \int_\Omega \frac{1}{2}\hat{\rho}_s\phi_s\left(\hat{k}_1\phi_s^2 + \hat{k}_2|\widehat{\nabla}\phi_s|^2\right)\mathrm{d}\hat{x} \tag{12}$$

is a special case of the well-known Ginzburg–Landau energy functional that is often used in statistical physics. It also coincides with the weighted $H^1(\Omega)$-norm of ϕ_s which naturally arises as the energy norm in many physical problems.

At this point, it is worth mentioning that experimental studies on granular materials suggest that there is a critical value ϕ_c such that for $\phi_s > \phi_c$ shearing of the material causes expansion, while for $\phi_s < \phi_c$ it causes contraction [2]. Intuitively, ϕ_c is the critical value of the solid volume fraction below which the grains are not expected to be in contact. This implies that the configuration pressure $\hat{\beta}_s$ should be zero, or generally *negligible*, for $\phi_s < \phi_c$. The value of ϕ_c depends on the geometries and size distribution of the solid particles. Therefore, the accurate calculation of this value constitutes a complicated topological problem. Nonetheless, for the simplest possible case, uniform spherical particles, a good estimate is $\phi_c \approx 0.52$. This number arises as the solution of the well-known inverse sphere packing problem in an equidistant lattice. It follows that a more realistic constitutive relation for the configuration pressure $\hat{\beta}_s$ would be the following,

$$\hat{\beta}_s = \begin{cases} \hat{k}_1\hat{\rho}_s(\phi_s - \phi_c)^2, & \phi_s \geqslant \phi_c, \\ 0, & \text{elsewhere}. \end{cases}$$

We remark, however, that since $\hat{\beta}_s$ appears only as a source term in (3), its precise functional form has no impact in our analysis and algorithm development, for as long as $\hat{\beta}_s$ remains bounded. Therefore, and for the sake of simplicity, we will assume that $\hat{\beta}_s$ is given by (11), unless otherwise stated.

Further, as regards the system of equations in hand, we observe that the solid phase density is a function of the solid pressure only, $\hat{\rho}_s = F(\hat{p}_s)$, because at equilibrium the temperature is constant and uniform. This implies that the only unknowns in the equilibrium equations are the solid volume fraction ϕ_s and the phasial pressures $\hat{p}_f, \hat{p}_s$. However, the distribution of the fluid pressure $\hat{p}_f$ can be written in analytic form after straightforward integration of Eq. (2),

$$\hat{p}_f = \hat{p}_0 e^{-\frac{|\mathbf{g}|}{R_f T}\hat{z}}, \tag{13}$$

where $\hat{p}_0$ is the fluid pressure at the ground level $\hat{z} = 0$, and $|\mathbf{g}|$ is the amplitude of the gravity vector $\mathbf{g}$.

Next, we introduce the difference of the phasial pressures $\hat{p}$,

$$\hat{p} = \hat{p}_s - \hat{p}_f = \hat{p}_s - \hat{p}_0 e^{-\frac{|\mathbf{g}|}{R_f T}\hat{z}} \tag{14}$$

and rewrite the equilibrium equations as

$$\widehat{\nabla}(\hat{p}\phi_s) = -\widehat{\nabla}\cdot(\hat{k}_2\hat{\rho}_s\phi_s\widehat{\nabla}\phi_s \otimes \widehat{\nabla}\phi_s) - \phi_s(\hat{\rho}_s - \hat{\rho}_f)\hat{\mathbf{g}}, \tag{15}$$

$$\hat{p} = \hat{k}_1\hat{\rho}_s\phi_s^2 - \widehat{\nabla}\cdot(\hat{k}_2\hat{\rho}_s\phi_s\widehat{\nabla}\phi_s). \tag{16}$$

This system has to be solved for ϕ_s and $\hat{p}$. Once $\hat{p}$ is known, the solid pressure $\hat{p}_s$ is calculated via (13) and (14). It is useful to remark that since $\hat{p}$ is merely the difference of the phasial pressures, it is not subject to any positivity constraint.

2.1. Ellipticity

Henceforth, we limit ourselves to $n = 2$, *i.e.*, we are going to study the two-dimensional problem in the XZ-plane, while taking into account the presence of gravitational forces. Nonetheless, the analysis can be applied to the three-dimensional case too, after certain minor modifications.

First, we observe that Eqs. (15) and (16) are quasilinear both in terms of ϕ_s and in terms of $\hat{p}$. This follows directly from the expressions of $\hat{\beta}_s$ and Γ_s in (8) and, in particular, from the independence of $\hat{\beta}_s$ and $\widehat{\Gamma}_s$ on $\widehat{\nabla}\phi_s$. Next, assuming that $\hat{p}$ is given as a source term, we identify in (16) the classical quasilinear modified Helmholtz equation in terms of the volume fraction ϕ_s. The required ellipticity follows if we observe that $\widehat{\Gamma}_s$, which is also the coefficient of the elliptic operator in (16), is by definition non-negative and uniformly bounded. Thus, Eq. (16) is elliptic with respect to ϕ_s. In order to show that the vector Eq. (15) is elliptic, we first introduce the decomposition

$$\widehat{\nabla}\cdot(\hat{k}_2\hat{\rho}_s\phi_s\widehat{\nabla}\phi_s\otimes\widehat{\nabla}\phi_s) = \widehat{\nabla}\cdot(\hat{k}_2\hat{\rho}_s\phi_s\widehat{\nabla}\phi_s)\cdot\widehat{\nabla}\phi_s + \hat{k}_2\hat{\rho}_s\phi_s H(\phi_s)\widehat{\nabla}\phi_s,$$

where $H(\phi_s)$ stands for the Hessian matrix of ϕ_s. Applying this decomposition to (15) and further assuming that $\partial\phi_s/\partial\hat{x}\neq 0$ and $\partial\phi_s/\partial\hat{z}\neq 0$, we arrive in the following system of equations,

$$\hat{p} + \phi_s\frac{\partial\hat{p}/\partial\hat{x}}{\partial\phi_s/\partial\hat{x}} + \widehat{\nabla}\cdot(\hat{k}_2\hat{\rho}_s\phi_s\widehat{\nabla}\phi_s) + \hat{k}_2\hat{\rho}_s\phi_s\left(\frac{\partial^2\phi_s}{\partial\hat{x}^2} + \frac{\partial^2\phi_s}{\partial\hat{x}\partial\hat{z}}\right) = 0,$$

$$\hat{p} + \phi_s\frac{\partial\hat{p}/\partial\hat{z}}{\partial\phi_s/\partial\hat{z}} + \widehat{\nabla}\cdot(\hat{k}_2\hat{\rho}_s\phi_s\widehat{\nabla}\phi_s) + \hat{k}_2\hat{\rho}_s\phi_s\left(\frac{\partial^2\phi_s}{\partial\hat{z}^2} + \frac{\partial^2\phi_s}{\partial\hat{x}\partial\hat{z}}\right) = -\frac{\phi_s(\hat{\rho}_s-\hat{\rho}_f)\hat{g}}{\partial\phi_s/\partial\hat{z}}.$$

Under the same reasoning as above for Eq. (16), the resulting system is elliptic in terms of ϕ_s. Therefore, given $\hat{p}\in L^2(\Omega)$, it follows from the convexity of the domain and the standard regularity lifting theorems that, whenever a solution ϕ_s exists, it belongs to the Sobolev space $H^i(\Omega), i\geqslant 1$ [18]. This smoothing result is not *a priori* obvious in equations describing equilibria of mixtures because of the definition of the volume fraction as an $L^1(\Omega)$ density, see Definition 2.0.1.

Further, we observe the presence of $\widehat{\rho_s}$ in the coefficients inside the differential operators of the system (15) and (16). But since $\widehat{\rho_s}$ and $\hat{p}$ are functionally dependent via the equation of state for the solid phase (6), then $\hat{p}$ enters explicitly the expression of the coefficients of the differential operators of the system. Thus, the system (15) and (16) is strongly coupled. Furthermore, this strong coupling is present even with the simplest possible equation of state for the solid phase, that of a stiffened gas. It is therefore, expected that more complicated equations of state will increase the complexity of the coupling.

In order to overcome the coupling that arises from the presence of the pressure $\hat{p}$ in the coefficients of the differential operators, we perform a perturbation analysis of the system (15) and (16), guided by standard scaling arguments of hydrostatics. Besides its usefulness for numerical purposes, this analysis provides physical insight on the relative contribution of each force to the equilibrium configuration of the mixtures of interest.

2.2. Perturbation analysis

First we write the system of Eqs. (15) and (16) in non-dimensional form. To this extent, we use the fluid pressure $\hat{p}_0$, and the fluid density $\hat{\rho}_0$, at ground level as reference values. Thus,

$$\hat{p}_s = \hat{p}_0 p_s, \quad \hat{p}_g = \hat{p}_0 p_g, \quad \widehat{P}_\infty = \hat{p}_0 P_\infty, \tag{17}$$

$$\hat{\rho}_s = \hat{\rho}_0\rho_s, \quad \hat{\rho}_g = \hat{\rho}_0\rho_g. \tag{18}$$

Further, the temperature $\widehat{T}$ is non-dimensionalized via the state equation of the fluid (5)

$$\widehat{T} = \frac{\hat{p}_0}{R_f\hat{\rho}_0}T. \tag{19}$$

Since the temperature is constant at equilibrium, we have $T = 1$ everywhere.

Moreover, the spatial variables $\hat{x},\hat{z}$ are non-dimensionalized by the characteristic length of the domain Ω, L_{ref}.

$$\hat{x} = L_{ref}x, \quad \hat{z} = L_{ref}z. \tag{20}$$

It is important to note that L_{ref} is assumed to be orders of magnitude larger than the characteristic length-scale of the grains, a necessary condition for the continuum hypothesis to be valid. Also, the constants $\hat{k}_1,\hat{k}_2$ are non-dimensionalized as follows,

$$\hat{k_1} = |\mathbf{g}|L_{ref}k_1, \quad \hat{k}_2 = |\mathbf{g}|L_{ref}^3k_2. \tag{21}$$

Finally, we define the parameter $\epsilon > 0$,

$$\epsilon = \frac{|\mathbf{g}|L_{ref}}{\hat{p}_0/\hat{\rho}_0}. \tag{22}$$

With the above non-dimensionalization, the equilibrium equations are written in the following, non-dimensional, form

$$\nabla(p\phi_s) = -\epsilon(\nabla\cdot(k_2\rho_s\phi_s\nabla\phi_s\otimes\nabla\phi_s) + \phi_s(\rho_s-\rho_f)\mathbf{z}), \tag{23}$$

$$p = \epsilon(k_1\rho_s\phi_s^2 - \nabla\cdot(k_2\rho_s\phi_s\nabla\phi_s)). \tag{24}$$

The system (23) and (24) is closed with the state equations in non-dimensional form. As mentioned above, for the non-dimensional temperature at equilibrium we have $T = 1$ everywhere. Thus, the non-dimensionalized equations of state at equilibrium read

$$p_f = \rho_f \tag{25}$$

and

$$p_s = -P_\infty + \frac{R_s}{R_f}\rho_s. \tag{26}$$

It is important to stress once again that these particular non-dimensional forms of the state equations are valid only for isothermal conditions, such as the equilibrium distributions considered herein. Finally, from Eq. (13) we obtain directly the analytical expression of the dimensionless fluid pressure p_f,

$$p_f = e^{-\epsilon z}. \tag{27}$$

Next, we observe that the denominator in (22), $\hat{p}_0/\hat{\rho}_0$, is at the order of magnitude of the square of the sound speed of the fluid phase. In turn, this implies that in most industrial applications and natural phenomena involving granular materials, the parameter ϵ is very small, *i.e.*, $\epsilon \ll 1$. In fact, since the denominator in (22) is typically at least as large as the acceleration of gravity, the parameter ϵ may be at the order of unity only if L_{ref} is very large. Such conditions, however, are highly unlikely to occur in equilibrium distributions of two-phase mixtures. One possible exception is a mixture whose fluid constituent is a rarefied gas (small $\hat{p}_0/\hat{\rho}_0$).

Such extreme cases, however, are beyond the scope of the present study. Thus, from now on we assume that ϵ is at least an order of magnitude smaller than unity. This, in turn, suggests that we can perform a perturbation expansion of the governing equations in powers of ϵ. Therefore, we assume the following, generally divergent, regular perturbation expansion,

$$p_s = p_s^0 + \epsilon p_s^1 + O(\epsilon^2), \tag{28}$$

$$p_f = p_f^0 + \epsilon p_f^1 + O(\epsilon^2), \tag{29}$$

$$\rho_s = \rho_s^0 + \epsilon\rho_s^1 + O(\epsilon^2), \tag{30}$$

$$\phi_s = \phi_s^0 + \epsilon\phi_s^1 + O(\epsilon^2). \tag{31}$$

By the uniqueness of the perturbation expansion we can easily obtain the perturbation expansions for the rest of the variables which appear as products and differences. For p we have

$$p = p^0 + \epsilon p^1 + O(\epsilon^2), \tag{32}$$

where $p^0 = p_s^0 - p_f^0$ and $p^1 = p_s^1 - p_f^1$ respectively. Similarly for $p\phi_s$ and $\rho_s\phi_s$ we have

$$p\phi_s = (p\phi_s)^0 + \epsilon(p\phi_s)^1 + O(\epsilon^2), \tag{33}$$

$$\rho_s\phi_s = (\rho_s\phi_s)^0 + \epsilon(\rho_s\phi_s)^1 + O(\epsilon^2), \tag{34}$$

where

$$(p\phi_s)^0 = p^0\phi_s^0,$$
$$(p\phi_s)^1 = p^0\phi_s^1 + p^1\phi_s^0,$$
$$(\rho_s\phi_s)^0 = \rho_s^0\phi_s^0,$$
$$(\rho_s\phi_s)^1 = \rho_s^0\phi_s^1 + \rho_s^1\phi_s^0.$$

Using exactly the same approach we can also obtain the expansions for triple products and higher-order products.

Inserting the expansions (28)–(34) to Eqs. (23) and (24), grouping terms of the same order and applying the fundamental theorem of perturbation theory [19], we obtain the following expressions for the zero-order terms,

$$p_f^0 = 1, \quad p_s^0 = 1, \tag{35}$$

$$\rho_f^0 = 1, \quad \rho_f^0 = (1+P_\infty)\frac{R_f}{R_s}, \tag{36}$$

$$\phi_s^0 + \phi_f^0 = 1 \tag{37}$$

and the following closed system of equations for the first-order terms,

$$p_f^1 = -z, \tag{38}$$

$$p^1 = k_1 \rho_s^0 (\phi_s^0)^2 - \nabla \cdot (k_2 \rho_s^0 \phi_s^0 \nabla \phi_s^0), \tag{39}$$

$$\nabla (p^1 \phi_s^0) = -\nabla \cdot (k_2 \rho_s^0 \phi_s^0 \nabla \phi_s^0 \otimes \nabla \phi_s^0) - \phi_s^0 \left(\rho_s^0 - \rho_f^0 \right) \mathbf{z}. \tag{40}$$

We observe that the coefficients of the differential operators in the perturbed system (39) and (40) do not depend on the pressure term p^1. Instead, only the (constant) zero-order solid density, ρ_s^0, enters the expressions for these coefficients. Therefore, the perturbation analysis has allowed us to overcome the problematic coupling caused by the presence of p in the coefficients of the differential operators and in β_s, in Eqs. (15) and (16). In other words, the perturbed system (39) and (40) is a fully decoupled set of PDEs.

Indeed, taking the gradient of (39) and combining with (40) results in the third-order vector equation for ϕ_s^0,

$$k_2 \rho_s^0 H(\phi_s^0) - \phi_s^0 \left(\rho_s^0 - \rho_f^0 \right) \mathbf{z} = -k_2 \rho_s^0 \phi_s^0 \nabla \left(\nabla \cdot \left(\nabla (\phi_s^0)^2 \right) \right) + 3 k_1 \rho_s^0 (\phi_s^0)^2 \nabla \phi_s^0. \tag{41}$$

This equation is obviously independent of p^1. The study of existence and regularity of (41) is by itself an important step towards a better understanding of the equilibrium behavior of granular mixtures and it will be addressed in a future work.

Further, we note that the saturation condition is preserved by ϕ_s^0 and ϕ_f^0. In addition, ϕ_s^0 obeys Eq. (40) which has the same structure as its unperturbed equivalent (16). We therefore conclude that ϕ_s^0 inherits the properties of ϕ_s and, particularly, it is also a probability density. On the other hand, the higher-order terms of the perturbation expansion of ϕ_s are not probability densities. Since in our study we will be dealing with the perturbed problem, we will refer to ϕ_s^0 as the "solid volume fraction".

Finally, we observe that the decoupling resulted from the perturbation analysis depends only on the denominator of (22), $\hat{p}_0/\hat{\rho}_0$, being large, under the isothermal conditions of thermodynamic equilibrium. Therefore, the analysis presented above is independent of the choice of the solid phase equation of state. Indeed, a different choice of state equation would result to the same perturbed problem, since the pressure $\hat{p}_s$ would still be a function of $\hat{\rho}_s$ only.

2.3. Integrability analysis

We observe that the governing system (15) and (16) is overdetermined in spatial dimensions higher than one. Moreover, the overdeterminacy carries over to the perturbed system (39) and (40) as well. Overdetermined systems of PDEs need to be supplemented with compatibility conditions which are generally difficult to obtain. At first sight, this might seem odd and give the impression that the system (15) and (16) and its perturbed version (39) and (40) are ill-posed. However, this is not the case.

In fact, in our case the overdeterminacy stems from the momentum equation (15) and is explained as follows. The momentum equation is a vector equation that expresses the balance of forces in each spatial dimension.On the other hand, at equilibrium it degenerates to an equation for the solid pressure, which is a scalar. However, since the momentum equation (15) has a clear physical meaning (balance of forces), the compatibility condition for the system (39) and (40) arises naturally and is remarkably simple.

It is also useful to remark that in mathematical terminology, this means that the system (39) and (40) is supplemented with a set of compatibility conditions so as the corresponding De Rham complex be exact. (By definition, the De Rham complex is exact if and only if its cohomologies are zero or, in the worst case, are finite dimensional, [20]). In turn, as shown in [20], exactness of the De Rham complex implies Frobenius integrability and solvability.

In fact, since the system (39) and (40) is decoupled, ϕ_s^0 can be obtained by solving Eq. (41). This equation is also overdetermined, but it is integrable by construction. Indeed, the symmetry of the higher-order mixed derivatives is satisfied identically, as one can verify by simple cross-differentiation. Once ϕ_s^0 is known, the unknown variable p^1 can be obtained via Eq. (40). We observe that this is an equation of the form

$$\nabla f = g. \tag{42}$$

It is well known, see for example [22], that Eq. (40) is integrable if and only if

$$-\nabla \cdot (k_2 \rho_s^0 \phi_s^0 \nabla \phi_s^0 \otimes \nabla \phi_s^0) - \phi_s^0 \left(\rho_s^0 - \rho_f^0 \right) \mathbf{z} \in \mathrm{Ker}(\mathrm{curl}). \tag{43}$$

In other words, Eq. (40) is integrable if and only if its right-hand side is curl-free. This necessary and locally sufficient condition follows formally by the fact that the De Rham complex is locally exact for the gradient operator [22].

To put it simply, condition (43) says that, assuming f to be smooth, the equality of the mixed second-order derivatives of f must carry over to the right-hand side of (42), thus, resulting in (43). We also remark that since the right-hand side of (40) stands for the source term g of Eq. (42), its precise functional form does not affect the integrability condition (43).

Next, let us assume that

$$-\nabla \cdot (k_2 \rho_s^0 \phi_s^0 \nabla \phi_s^0 \otimes \nabla \phi_s^0) - \phi_s^0 \left(\rho_s^0 - \rho_f^0 \right) \mathbf{z} \in L^{2,2}(\Omega) \tag{44}$$

and recall the well-known Helmholtz decomposition,

$$L^{2,2}(\Omega) = L^{2,2}_{\mathrm{div}}(\Omega) \oplus L^{2,2}_{\mathrm{curl}}(\Omega), \tag{45}$$

where $L^{2,2}_{\mathrm{div}}(\Omega)$ is the space of the *solenoidal* vector fields, *i.e.*, divergence-free vector fields obeying a no-slip condition in the boundary. Also, in (45), $L^{2,2}_{\mathrm{curl}}(\Omega)$ is the orthogonal complement of $L^{2,2}_{\mathrm{div}}(\Omega)$, *i.e.*, the space of curl-free vector fields that can be expressed in the form of a potential. By virtue of the Helmholtz decomposition and of assumption (44), the integrability condition (43) can be reformulated as

$$-\nabla\cdot\left(k_2\rho_s^0\phi_s^0\nabla\phi_s^0\otimes\nabla\phi_s^0\right) - \phi_s^0\left(\rho_s^0-\rho_f^0\right)\mathbf{z} \in L^{2,2}_{\mathrm{curl}}(\Omega). \tag{46}$$

Therefore, we have, in a sense, the reciprocal of the Leray projector [23] used in the incompressible Navier–Stokes equations. The curl-free part of an $L^{2,2}$-vector field can be uniquely determined, up to an additive constant, via the use of Ladyzhenskaya's theorem [24], which states that:

Theorem 2.3.1 (Ladyzhenskaya's theorem). *Given an $L^{2,2}$-vector field F in Ω, its curl-free part is the solution of the Neumann problem,*

Find $u \in H^1(\Omega)$ such that

$$\nabla\cdot(\nabla u) = \nabla\cdot(F) \quad \text{in } \Omega,$$
$$\frac{\partial u}{\partial n} = \frac{\partial F}{\partial n} \quad \text{in } \partial\Omega.$$

With the use of Ladyzheskaya's theorem, we apply the divergence operator in all terms of (40) which transforms it to the following equivalent Poisson equation with Neumann data,

$$\nabla\cdot\left(\nabla\left(p^1\phi_s^0\right)\right) = -\nabla\cdot\left(\nabla\cdot\left(k_2\rho_s^0\phi_s^0\nabla\phi_s^0\otimes\nabla\phi_s^0\right) + \phi_s^0\left(\rho_s^0-\rho_f^0\right)\mathbf{z}\right) \quad \text{in } \Omega, \tag{47}$$

$$\nabla\left(p^1\phi_s^0\right)\cdot\mathbf{n} = -\left(\nabla\cdot\left(k_2\rho_s^0\phi_s^0\nabla\phi_s^0\otimes\nabla\phi_s^0\right) + \phi_s^0\left(\rho_s^0-\rho_f^0\right)\mathbf{z}\right)\cdot\mathbf{n} \quad \text{in } \partial\Omega. \tag{48}$$

The main advantage of Ladyzhenskaya's theorem is that it allows us to overcome the overdeterminacy of the momentum equation (40) by projecting the right-hand side of (40) to the correct space. Moreover, the new equation is equivalent to the original one, thus, no information is lost from this projection. Further, it provides compatibility conditions on the boundary for both the volume fraction ϕ_s and the pressure difference p. Finally, it can be extremely useful for numerical purposes because it transforms the momentum equation to a Poisson equation, which can be easily treated numerically.

At this point it is important to mention that the system in hand admits *multiple* solutions even after imposing compatibility conditions. This non-uniqueness implies that the two-phase mixtures of interest can support multiple equilibrium distributions. This, in turn, implies that the equations of the full model that describe the evolution of the mixture towards equilibrium, see Appendix, constitute a non-ergodic dynamical system since ergodicity is equivalent with the existence and uniqueness of an equilibrium distribution, [21]. In fact, since an equilibrium distribution is the large-time solution of the initial-boundary value problem associated with the full model, it depends strongly on the initial conditions.

Further,by Ladyzhenskaya's theorem and by the existence and uniqueness results for the Neumann problem of the Poisson equation [18], it follows that for every smooth solution of (41) ϕ_s^0, we obtain only one, up to a constant, equilibrium pressure distribution. This implies that the perturbed problem admits an one-parameter family of solutions. Thus, we arrive to the important conclusion that non-physical solutions, such as two different pressure distributions corresponding to the same volume fraction distribution, are not admitted by the system of equations in hand.

3. The numerical method

As mentioned earlier, Ladyzhenskaya's theorem can be used in the design of a projection method for the computation of p^1 from the momentum equation (40). This implies that ϕ_s^0 must be computed first. One method to perform the computation of ϕ_s^0 is to solve numerically Eq. (41). Nonetheless, this is a third-order vector equation and, therefore, its numerical approximation is cumbersome.

A more efficient and robust method is to compute ϕ_s^0 from the compaction equation (39), which is the method adopted herein. This suggests the use of a successive-over-relaxation (SOR) method for the compaction equation (39) via the introduction of a pseudo-temporal derivative and, thus, by the transformation of the original boundary problem to a Cauchy problem. The desired solution is then the steady-state solution of the initial value problem. The temporally relaxed compaction equation has the form

$$\frac{\partial\phi_s^0}{\partial t} = p^1 - k_1\rho_s^0\left(\phi_s^0\right)^2 + \nabla\cdot\left(k_2\rho_s^0\phi_s^0\nabla\phi_s^0\right). \tag{49}$$

The temporally relaxed compaction equation (49) is an equation of reaction–diffusion type, *i.e.*, an equation of the form

$$\frac{\partial u}{\partial t} = \triangle u^m - u^p.$$

Such equations are often encountered, among other applications, in models of flows through porous media, [25,26].

In our case, the variable u is the solid volume fraction, which is positive and bounded, $\phi_s^0 \in [0,1]$. This fact and the convexity of β_s^0 with respect to ϕ_s^0 imply that blow-up of the classical-strong solutions is not to be expected. The temporal relaxation of ϕ_s^0 further implies the temporal relaxation of p^1 due to the coupling between (39) and (40).

Due to its simplicity and straightforward implementation we employ the second approach for the numerical solution of the system. Summing up, the proposed numerical method consists of the following major steps,

(i) Predictor–corrector SOR algorithm for the compaction equation (39).
(ii) Predictor–corrector projection method, based on Ladyzhenskaya's theorem for the momentum equation (40).

The use of a predictor–corrector algorithm is motivated by the fact that such methods are well known for their stability and robustness in non-linear parabolic equations [27]. Also, such methods have been successfully applied to systems containing stiff reaction diffusion equations [28].

3.1. Spatio-temporal discretization and flow-chart of the algorithm

In order to simplify the algebra, and without loss of generality, we assume that Ω is discretized via an equidistant mesh $T_{\Delta x,\Delta y}$ with mesh size $\Delta x = \Delta y$, *i.e.*, $T_{\Delta x,\Delta y} = T_{\Delta x}$. Also, following standard practices, we assume that $T_{\Delta x}$ is equipped with a lexicographic ordering relation. Further, $T_{\Delta x}$ is assumed to consist of $N \times M$ grid points, N generally being non-equal to M. Finally, we adopt the following notation convention:

- The superscripts $n, n+1$ denotes the *corrected* values in times $t_n = n\Delta t$ and $t_{n+1} = (n+1)\Delta t$ respectively.
- The superscript * refers to the predicted value in the time step t_n.
- Spatial coordinates are represented as ordered sub-indices $\{ij\}$.
- All differential operators appearing in the flow-chart of the algorithm are assumed to be *finite difference operators*.
- Due to the presence of multiple superscripts, we drop the exponents 0 and 1 from ϕ_s^0 and p^1, respectively, without risk of confusion.

In the proposed algorithm, spatial differential operators are discretized via 2nd-order accurate, central finite differences. space. Further, temporal differential operators are discretized via forward finite differences, with time step $\Delta t \leqslant F(\Delta x)$. As usual, the function F will be calculated during the stability analysis. The use of forward finite differences reflects the fact that Eq. (39) is parabolic, hence central or backward differences offers no advantage. Finally, we define the function $\mathrm{Res}(p^i, \phi^i)$ as follows:

$$\mathrm{Res}\left(p^i, \phi_s^i\right) = p^i - k_1 \rho_s^0 \left(\phi_s^i\right)^2 + \nabla \cdot \left(k_2 \rho_s^0 \phi_s^i \nabla \phi_s^i\right), \quad i = n, n+1, *. \tag{50}$$

The flow-chart of the algorithm is the following.

3.1.1. Prediction step

1. The predicted value ϕ_s^* of the volume fraction in the $(n+1)$th step is computed from the compaction equation as follows:

$$\frac{\phi_s^* - \phi_s^n}{\Delta t} = \mathrm{Res}\left(p^n, \phi_s^n\right). \tag{51}$$

2. The predicted value p^* is computed by taking the divergence of (40), solving the resulting Neumann problem of the Poisson equation for the product $(p\phi_s)$,

$$\nabla \cdot (\nabla (p\phi_s)^*) = -\nabla \cdot (\nabla \cdot \left(k_2 \rho_s^0 \phi_s^* \nabla \phi_s^* \otimes \nabla \phi_s^*\right) - \phi_s^* \left(\rho_s^0 - \rho_f^0\right)\mathbf{g}), \tag{52}$$

$$\nabla (p\phi_s)^* \cdot \mathbf{n} = -\nabla \cdot \left(k_2 \rho_s^0 \phi_s^* \nabla \phi_s^* \otimes \nabla \phi_s^*\right) - \phi_s^* \left(\rho_s^0 - \rho_f^0\right)\mathbf{z} \cdot \mathbf{n} \tag{53}$$

and then dividing by ϕ_s^*.

3.1.2. Correction step

1. The corrected value ϕ_s^{n+1} of the volume fraction in the $(n+1)$th step is computed from the compaction equation as follows:

$$\frac{\phi_s^{n+1} - \phi_s^n}{\Delta t} = \mathrm{Res}(p^*, \phi_s^*). \tag{54}$$

2. The corrected value p^{n+1} is computed by taking the divergence of (40), solving the resulting Neumann problem of the Poisson equation,

$$\nabla \cdot (\nabla (p\phi_s)^{n+1}) = -\nabla \cdot \left(\nabla \cdot \left(k_2 \rho_s^0 \phi_s^{n+1} \nabla \phi_s^{n+1} \otimes \nabla \phi_s^{n+1} \right) - \phi_s^{n+1} \left(\rho_s^0 - \rho_f^0 \right) \mathbf{z} \right), \tag{55}$$

$$\nabla (p\phi_s)^{n+1} \cdot \mathbf{n} = -\left(\nabla \cdot \left(k_2 \rho_s^0 \phi_s^{n+1} \nabla \phi_s^{n+1} \otimes \nabla \phi_s^{n+1} \right) \right) \cdot \mathbf{n} - \phi_s^{n+1} \left(\rho_s^0 - \rho_f^0 \right) \mathbf{z} \cdot \mathbf{n} \tag{56}$$

and then dividing by ϕ^{n+1}.

4. Stability, consistency and convergence

In this section we present the stability and consistency analysis of the proposed numerical method. The numerical solutions that the method produces in the various time-steps are interpreted as vectors, according to the lexicographic relation that $T_{\Delta x}$ is equipped with. Moreover, for reasons concerning the invertibility of operators, we will assume that $N = M$.

Solutions throughout this section are understood as strong solutions with "sufficient smoothness" in space and time. As usual, and for the sake of simplicity, the analysis focuses on the pure Cauchy problem with periodic boundary conditions. The following notation convention for the discrete version of the spatial differential operators is adopted.

- $M(\phi_s)$ denotes the finite difference operator that approximates
  $\nabla \cdot \left(k_2 \rho_s^0 \phi_s \nabla \phi_s \right)$.
- $A(\phi_s)$ denotes the finite difference operator that approximates
  $\nabla \cdot \left(-\nabla \cdot \left(k_2 \rho_s^0 \phi_s \nabla \phi_s \otimes \nabla \phi_s \right) \right)$.
- $B(\phi)$ denotes the finite difference operator that approximates
  $\nabla \cdot \left(\phi_s \left(\rho_s^0 - \rho_f^0 \right) \mathbf{z} \right)$.

Finally, due to the use of the multiples sub-indices in the representation of ϕ_s as a vector, we drop the subscript s, *i.e.*, $\phi_s = \phi$, without the risk of confusion.

4.1. Stability

We begin the stability analysis of the numerical method by proving the following lemmas.

Lemma 4.1.1. *Let*

$$F : [0,1]^{N^2} \times \mathbb{R}^{N^2} \to \mathbb{R}^{N^2},$$
$$(\phi^n, p^n) \mapsto \phi^*$$

denote the non-linear function of the iteration equation

$$\phi^* = F(\phi^n, p^n),$$

defined through the spatio-temporal discretization of the temporally relaxed compaction equation (49). Then, F is globally Lipschitz, with Lipschitz constant

$$K(\Delta x, \Delta t) = \|D(F)\|_\infty, \tag{57}$$

where $D(F)$ is the first-order Frechet derivative of F.

Proof. The function F, see (51), has the coordinate-wise analytical expression,

$$\phi_{ij}^* = \phi_{ij}^n - \frac{\Delta t}{2} k_1 \rho_s^0 \left(\phi_{ij}^n \right)^2 + \frac{\Delta t}{2} p_{ij}^n + \frac{\Delta t}{2} \sum_{k=1}^{N^2} M_{ij,k}(, \phi^n).$$

We observe that F is continuously differentiable, as a multi-variable non-linear function of polynomial type and, therefore, it is locally Lipschitz. To prove that it is globally Lipschitz it suffices to bound the first-order Frechet derivative $D(F)$ in the sup-norm. That is, we have to bound the following quantity

$$\|D(F)\|_\infty = \sup \left\{ \sum_{k=1}^{N^2} |J(F)_{ij,k}| \right\},$$

where $J(F)$ stands for the Jacobian matrix of F. The analytical expression of the rows of $J(F)$ depends only on whether the specific row corresponds to a grid point whose neighbors involve the boundary. The proof follows if we observe that F is linear with respect to p_{ij}^n, hence, p_{ij}^n is represented as constant in the Jacobian, and that the non-linear (polynomial) terms, take values in bounded domains. The Lipschitz constant K due to the continuous differentiability of F reads

$$K(\Delta(x), \Delta(t)) = \|D(F)\|_\infty,$$

which completes the proof of the lemma. □

Lemma 4.1.2. *Assume that $\phi^n \in [0,1]^{N^2}$. Then, there exists a constant $C = C(\Delta(x))$ such as*

$$\|p_{ij}^n\|_{\max} \leqslant C\|\phi_{ij}^n\|_{\max}.$$

Proof. The right-hand side of the Poisson equation (48) is approximated by the operators $A(\phi^n)$ and $B(\phi^n)$. In fact, $A(\phi^n)$ is a matrix and each of its elements is a polynomial function of ϕ^n in the domain $[0,1]^{N^2}$. By standard continuity arguments there exists a constant $C_1 = C_1(\Delta x)$ such that

$$A_{k,l}(\phi^n) \leqslant C_1\|\phi^n\|_{\max} \quad \forall\{k,l\}. \tag{58}$$

Moreover, $A(\phi^n)$ is of the form $A(\phi^n) = \frac{1}{\Delta x^4}\widetilde{A}(\phi^n)$, where $\widetilde{A}(\phi^n)$ is an operator which does not depend on Δx. Thus, $C_2 = \frac{1}{\Delta x^4}C_1$ and (58) becomes

$$A_{k,l}(\phi^n) \leqslant \frac{C_2}{\Delta x^4}\|\phi^n\|_{\max} \quad \forall\{k,l\}. \tag{59}$$

Analogously, for $B(\phi^n)$ we have that there exists a constant C_3 such as

$$B_{k,l}(\phi_n) \leqslant \frac{C_3}{\Delta x}\|\phi^n\|_{\max} \quad \forall\{k,l\}. \tag{60}$$

Now, let $L/\Delta x^2$ denote the finite difference operator that discretizes the Laplacian in the left hand side of (48). L is a tri-diagonal matrix whose element do not depend on Δx. From (59) and (60) we have

$$\|(p\phi)^n\|_{\max} \leqslant \|L^{-1}\|_\infty \frac{C_2}{\Delta x^2}\|\phi^n\|_{\max}.$$

Since ϕ^n, is bounded there exists a constant C_4 such as

$$C_4\|p^n\|_{\max} \leqslant \|(p\phi)^n\|_{\max} \leqslant \|L^{-1}\|_\infty\left(\frac{C_2}{\Delta x^2} + C_3\Delta x^3\right)\|\phi^n\|_{\max},$$

therefore,

$$\|p^n\|_{\max} \leqslant C(\Delta x)\|\phi^n\|_{\max},$$

where $C(\Delta x) = \|L^{-1}\|_\infty(\frac{C_2}{\Delta x^2} + C_3\Delta x^3)$ and thus the proof is completed. □

We can now prove the stability theorem.

Theorem 4.1.3. *Let ϕ^n, ϕ^*, p^n, p^* stand for the predicted and corrected solution vectors that are obtained in the nth step. Assume that $\phi^0 \in [0,1]^{N^2}$, where ϕ^0 is the initial condition of the volume fraction. Then if the following condition holds,*

$$K(\Delta(x), \Delta(t))(1 + C(\Delta x)) \leqslant 1, \tag{61}$$

the numerical method is stable.

Proof. First we show the stability of (51). From Lemmas 4.1.1 and 4.1.2 we have

$$\|\phi^*\|_{\max} \leqslant K(\Delta(x), \Delta(t))(1 + C(\Delta x))\|\phi^n\|_{\max}.$$

Now, fix $n = 0$. By the theorem's assumption on the initial conditions we have that

$$\|\phi^*\|_{\max} \leqslant K(\Delta(x), \Delta(t))(1 + C(\Delta x)),$$

therefore, if

$$K(\Delta(x), \Delta(t))(1 + C(\Delta x)) \leqslant 1, \tag{62}$$

we have that $\|\phi^*\|_{\max} \leqslant 1$. Since the prediction and correction steps have the same structure, we also have $\|\phi^1\|_{\max} \leqslant 1$. Induction completes the proof for arbitrary n.

The stability of the Poisson equation (48) follows from the stability of the finite difference approximation [29]. □

Apart from the stability properties of the proposed algorithm it is important to show that the non-linear function F is positivity preserving, *i.e.*, it maps probability densities to probability densities. To this extent, we first observe that condition (62) is of the form $\Delta t \leqslant G_1(\Delta x)$.

In fact, positivity of ϕ^* and, thus of ϕ^{n+1}, follows by repeating the steps in the proofs of Lemmas 4.1.1 and 4.1.2. In this case, however, one must drop the absolute values and replace (62) by the similar condition $\Delta t \leqslant G_2(\Delta x)$. In other words, we have shown the following.

Proposition 4.1.4. *Assume that Δx are chosen so as $G_1(\Delta x)$ and $G_2(\Delta x)$ are strictly smaller than one. Further, let $G(\Delta x) = \min\{G_1(\Delta x), G_2(\Delta x)\}$. Then, if*

$$\Delta t \leqslant G(\Delta x), \tag{63}$$

the function $F : [0,1]^{N^2} \times \mathbb{R}^{N^2} \to \mathbb{R}^{N^2}$ is positivity preserving.

Eq. (63) states the condition that must be satisfied by Δt and Δx so as for the numerical method to be stable and positivity preserving. A rough computation shows that, asymptotically, Eq. (63) has the analytical form $\Delta t \leqslant \Delta x \min\{k_1, k_2\}$. The exact formulation for arbitrary Δx and Δt, throughout this approach is very challenging for two reasons. First, (63) is rational in its arguments and, therefore, one needs to perform a series of complicated algebraic manipulations in order to transform it into a more manageable form. Second, calculation of the optimal constants is not straightforward. To see this, we recall that each row of the matrices A and $B_{i,j}$ gives rise to non-linear polynomial functions of the ϕ_{ij} arguments. Therefore, the optimal constants for the bounds obtained in Theorem 4.1.3 and Proposition 4.1.4 are the solutions to the corresponding non-linear optimization problems over the unit N^2-dimensional cube. However, solving such problems is far from trivial and, in any case, time-consuming.

In our case it is sufficient to use the asymptotical formulation $\Delta t \leqslant \Delta x \min\{k_1, k_2\}$, which corresponds to a *feasible* solution of the non-linear optimization problem. This feasible solution can be obtained easily due to the special structure of the domain.

4.2. Consistency

The consistency of the numerical method is demonstrated in the following theorem.

Theorem 4.2.1. *Let us assume the conditions of Theorem 4.1.3, Proposition 4.1.4 and that the condition (63) is satisfied. Further, we assume that the unique solution pair $\phi(x,t), p(x,t)$ of the Cauchy problem with initial data $\phi^0 = \phi(x,0)$ and $p^0 = p(x,0)$ in the range $(0,T)$ has the following properties,*

1. $\phi(x,t) \in C^3((0,T) : C^3(\Omega))$,
2. $p(x,t) \in C^3((0,T) : L^2(\Omega))$,
3. $p\phi \in C^3((0,T) : H^2(\Omega))$.

Then, the numerical method proposed is consistent both in space and in time.

Proof. As usual, we will treat spatial and temporal consistency separately. First we show temporal consistency by assuming that the method is exact in the spatial level. Assuming that the method is exact in the time step n, the local truncation error reads in the time-step $n+1$

$$\|\phi^{n+1} - \phi(t_{n+1})\|_{\max} = \|\phi^{n+1} + \phi^* - \phi^* - \phi(t_{n+1})\|_{\max} \leqslant \|\phi^* - \phi(t_{n+1})\|_{\max} + \|\phi^{n+1} - \phi^*\|_{\max}. \tag{64}$$

We will treat the two components of (64) separately.

For the first component of (64), $\|\phi^* - \phi(t_{n+1})\|_{\max}$, exact Taylor expansion of $\phi(t_{n+1})$ around t_n combined with the definition of ϕ^* in (51) gives

$$\|\phi^* - \phi(t_{n+1})\|_{\max} = \left\| \phi^n + \Delta t \mathrm{Res}(\phi^n, p^n) - \left(\phi(t_n) + \Delta t \frac{\partial \phi}{\partial t}(t_n) + \Delta t^2 \frac{\partial^2 \phi}{\partial t^2}(\xi)\right)\right\|_{\max},$$

where $\xi \in (t_n, t_{n+1})$. The assumption that the method is exact in the spatial level, and in the nth time-step, implies that

$$\left\| \phi^n + \Delta t \mathrm{Res}(\phi^n, p^n) - \left(\phi(t_n) + \Delta t \frac{\partial \phi}{\partial t}(t_n) + \Delta t^2 \frac{\partial^2 \phi}{\partial t^2}(\xi)\right)\right\|_{\max} \leqslant \left\| \Delta t^2 \frac{\partial^2 \phi}{\partial t^2}(\xi)\right\|_{\max}. \tag{65}$$

Since $\phi \in C^3((0,T) : C^3(\Omega))$ it follows that (65) can be bounded by

$$\left\| \Delta t^2 \frac{\partial^2 \phi}{\partial t^2}(\xi)\right\|_{\max} \leqslant \Delta t^2 \left\| \frac{\partial^2 \phi}{\partial t^2}\right\|_{C^3((0,T)\cdot C^3(\Omega))} = O(\Delta t^2). \tag{66}$$

For the second component of (64) $\|\phi^{n+1} - \phi^*\|_{\max}$ we have

$$\|\phi^{n+1} - \phi^*\|_{\max} = \Delta t \|\mathrm{Res}(\phi^*, p^*) - \mathrm{Res}(\phi^n, p^n)\|_{\max} = \Delta t \|k_1(\rho_s^0(\phi^*)^2 - \rho_s^0(\phi^n)^2) + (p^* - p^n) + M(\phi^*) - M(\phi^n)\|_{\max}$$
$$\leqslant \Delta t(\|k_1(\rho_s^0(\phi^*)^2 - \rho_s^0(\phi^n)^2)\|_{\max} + \|(p^* - p^n)\|_{\max}) + \Delta t \|M(\phi^*) - M(\phi^n)\|_{\max}. \quad (67)$$

We study the three components of (67) separately. For the component $\|(p^* - p^n)\|_{\max}$ we have,

$$\|((p\phi)^* - (p\phi)^n)\|_{\max} = \|A(\phi^n) - A(\phi^*) + B(\phi^n) - B(\phi^*)\|_{\max} \leqslant \|A(\phi^n) - A(\phi^*)\|_{\max} + \|B(\phi^n) - B(\phi^*)\|_{\max}.$$

The continuity of the functions $A(.,.), B(.,.)$ and (66) imply that as $\Delta t \to 0$ the following holds.

$$\|((p\phi)^* - (p\phi)^n)\|_{\max} \to 0.$$

This, in turn implies that

$$\|(p^* - p^n)\|_{\max} \to 0.$$

The rate of consistency follows from the rate of $\|\phi^* - \phi^n\|_{\max}$, *i.e.*,

$$\|(p^* - p^n)\|_{\max} = O(\Delta t^2). \quad (68)$$

Finally, (66) implies that

$$\|M(\phi^*) - M(\phi^n)\|_{\max} = O(\Delta t^2), \quad (69)$$
$$\|k_1(\rho_s^0(\phi^*)^2 - \rho_s^0(\phi^n)^2)\|_{\max} = O(\Delta t^2), \quad (70)$$

Summing up (68)–(70) we obtain

$$\|\phi^{n+1} - \phi^*\|_{\max} = O(\Delta t^2), \quad (71)$$

and therefore, combining (66) and (71) we have

$$\|\phi^{n+1} - \phi(t_{n+1})\|_{\max} = O(\Delta t^2).$$

Hence, the method is second-order consistent in time. Spatial consistency for $\phi, p\phi$ follows from the standard estimates for Poisson equations [29]. □

We conclude this section with the convergence corollary.

Corollary 4.2.2. *Under the assumptions of Theorems 4.1.3, 4.2.1 and Proposition 4.1.4 the discrete solution pair (ϕ^n, p^n) produced by the numerical method, converges to the unique solution pair of the Cauchy problem $(\phi(x,t), p(x,t))$ in the max-norm as $\Delta t, \Delta x \to 0$.*

Proof. The proof follows by the Lax–Richtmyer generalized equivalence principle for quasilinear systems. This, well known, principle states that stability and consistency imply convergence [30,31]. □

5. Remarks on the unperturbed problem

The numerical method that we propose is formally valid for the perturbed system (39) and (40), *i.e.*, when $\epsilon \ll 1$. Nonetheless, we have also applied the proposed algorithm to the unperturbed problem, in order to study the validity of the perturbation expansion derived in Section 2.2. The only modification that the algorithm requires is to update the density of the solid phase ρ_s, which is not constant. This is performed by solving the solid equation of state for ρ_s (6), immediately after the computation of the pressure difference p.

Our numerical experiments showed virtually no difference between the solutions of the original system (15) and (16) and its perturbed version (39) and (40). The agreement of these numerical results provides evidence for the validity of the perturbation expansion of Section 2.2.

Further, the numerical experiments showed that when $\epsilon \ll 1$, the solid density variations predicted by the unperturbed problem are negligible. This allows the direct application of the proposed method to the unperturbed problem. However, when ϵ grows larger, the solid density variations are no longer negligible. Also the unperturbed system (15) and (16) is endowed with a different set of compatibility conditions, which are given below. Therefore, the direct application of our numerical method to the unperturbed (15) and (16) without modification will might lead to incorrect results.

As mentioned earlier, the parameter ϵ is very small in all industrial applications and natural phenomena involving granular materials that we are aware of. However, the case where ϵ is not small is still interesting from the theoretical point of view (and possibly from the practical point of view as well, since this type of equations might arise in other areas of physical sciences). For this reason it is worth discussing possible ways to treat the governing system (15) and (16) numerically when ϵ is not small.

It is clear that in this case the perturbation expansion is no longer valid, unless the convergence of the expansion is formally proven. However, if ϵ is neither in the limit range of zero nor at the order of unity (for example, if $\epsilon = 0.15$) it is possible to extend the perturbation analysis via Padé approximation. This amounts to reconstruct the perturbation expansion as a series of Padé approximates. Such series are known to successfully approximate the corresponding functions for values of ϵ in the range 0.1–0.2; see, for example, [32]. Despite the obvious disadvantage of having to compute higher-order terms of the original perturbation expansion, the proposed numerical method can in principle be applied to the new perturbed problem, thanks to the constructive definition of the Padé coefficients.

Further, if $\epsilon = O(1)$, then the full, unperturbed, problem has to be considered. In this case, as we mentioned before, the presence of $\hat{p}$ in the coefficients of the differential operators results in a strongly coupled system of equations. As a consequence, the momentum equation (15) no longer takes the simple form $\nabla f = g$ and, therefore, the Helmholtz decomposition (45) is not helpful anymore. Instead, Eq. (15), in two dimensions, has the following form,

$$\left(\frac{\partial}{\partial x} + A_1(x,z)\right) f = \omega_1, \tag{72}$$

$$\left(\frac{\partial}{\partial z} + A_2(x,z)\right) f = \omega_2. \tag{73}$$

Such equations have been used as examples of the classical Frobenius integrability theorem. Their compatibility condition reads

$$\left(\frac{\partial}{\partial x} + A_1(x,z)\right) \omega_2 = \left(\frac{\partial}{\partial z} + A_2(x,z)\right) \omega_1, \tag{74}$$

which is the classical commutation relation accounted in Lie theory [33]. This new compatibility condition acts as a constraint on (72) and (73), thus taking care of the overdeterminacy problem.

However, the design of an algorithm for the numerical treatment of the new constrained system is much more challenging. This is because the new compatibility condition, (74), when combined with the Helmholtz decomposition (45), does not produce a simple condition for the right-hand sides of (72) and (73), contrary to the outcome of the perturbed case, see Eq. (46). Therefore, the momentum equation can no longer be transformed into an equivalent Poisson equation by simply applying the divergence operator. In this case, taking the divergence of the momentum equation will give rise to incompatibilities on the boundary.

A possible approach for the numerical treatment of the unperturbed problem is to simultaneously solve all equations, including the compatibility condition, via a Newton–Raphson method. However, the implementation of this approach is very challenging. The main difficulty of this approach comes from the discretization of the momentum equation. If one chooses one-sided finite differences for the approximation of the gradient operator, then the corresponding linear system is well-posed; however one order of accuracy is lost. This can be detrimental when the problem involves non-linear, high-order terms, like the tensor product of the gradients that appears in the expression for the residual stresses. On the other hand, if one chooses 2nd or higher-order central differences, as is often the case, then the corresponding linear system becomes ill-posed because the diagonal of the matrix has zeros everywhere. A possible straightforward way to overcome the ill-posedness of the linear-system is the use of Tikhonov regularization, [34]. This method, roughly speaking, transforms the linear system in a regularized least-square minimization problem. Further, with this approach certain classical technical difficulties of the Newton–Raphson method must be resolved, such as the analytic derivation of the corresponding Jacobian matrix and a judiciously chosen initial guess.

6. Numerical results

The efficiency of the proposed numerical method has been investigated in a series of numerical experiments, part of which will be presented in this Section. In these numerical experiments we have used a mixture of water and beach sand as the mixture of reference.

6.1. Set up of the numerical experiments

The first issue that arises in the numerical treatment of equations for granular mixtures is the values of the constants $\hat{k}_1$ and $\hat{k}_2$ in the free energy component $\hat{\psi}^{\xi}_{s}$; see Eq. (10). Ideally, for a given granular material, these values should be obtained experimentally. However, to the best of our knowledge, accurate experimental data for these parameters are not yet available. For this reason, we resorted in considering values from earlier numerical studies.

In particular, we have used the same physical parameters as the ones given by the authors in [2], who studied numerically shearing motions of a saturated water-beach sand mixture. These values are $\hat{k}_1 = 0.02\ \mathrm{m}^2/\mathrm{s}^2$ and $\hat{k}_2 = 4 \times 10^{-8}\ \mathrm{m}^4/\mathrm{s}^2$. It should be mentioned that the authors in [2] did not elaborate on how these values were prescribed. However, they noted that the acquisition of values for these parameters is problematic. The same values were later adopted in [6] who studied the same problem as in [2], but with a different constitutive model.

It should also be noted that the above value of $\hat{k}_2$ is very small. Indeed, a heuristic order of magnitude analysis of the momentum equation (40) shows that, with this choice of $\hat{k}_2$, the amplitude of the residual stresses $\hat{\boldsymbol{\sigma}}$ is three to five orders smaller than that of the gravitational forces $\phi_s(\hat{\rho}_s - \hat{\rho}_f)\hat{\mathbf{g}}$. For such small values of $\hat{k}_2$, the effect of the residual stresses on $\hat{p^1}\phi_s^0$ is expected to be non-negligible only inside boundary or transition layers. Since the limit $\hat{k}_2 \to 0$ is singular, solutions of the governing Eqs. (39) and (40), for such small values of $\hat{k}_2$, can also be studied via singular perturbation techniques.

For the sake of completeness, we also note that the extreme case where $\hat{k}_2 = 0$ admits solutions in closed form. This limit case, however, refers to granular materials that do no support shear at equilibrium and, therefore, has no physical interest.

For our simulations, the beach sand is assumed to obey the stiffened gas equation of state (6) with the correction pressure equal to $\hat{P}_\infty = 10^8$ atm. Further, the water is assumed to behave like a simple Newtonian fluid and, therefore, $\hat{\beta}_f = 0$, $\hat{\Gamma}_f = 0$. Further, the uniform temperature of the mixture $\hat{T}$ is set equal to 300 K. The computational domain is a square with sides equal to $L = 0.1$ m.

As mentioned in Section 2.2, the water pressure and density at ground level, $\hat{z} = 0$ m, are used as reference values. Thus, $\hat{p}_0 = 1$ atm and $\hat{\rho}_0 = 1000$ kg/ m^3. Also, we use the length of the side of the computational domain as characteristic length: $L_{ref} = 0.1$ m. With this choice of reference values, the perturbation parameter is $\epsilon \simeq 0.0098$. This is in fact a small value, as required for the validity of the perturbation expansion.

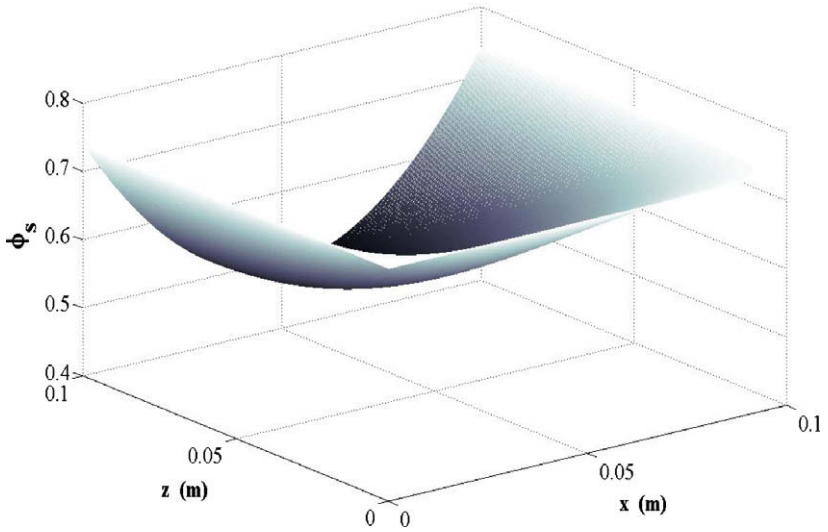

Fig. 1. Solid volume fraction $\phi_s^0, \hat{k}_1 = 0.02$ m^2/s^2, $\hat{k}_2 = 4 \times 10^{-8}$ m^4/s^2.

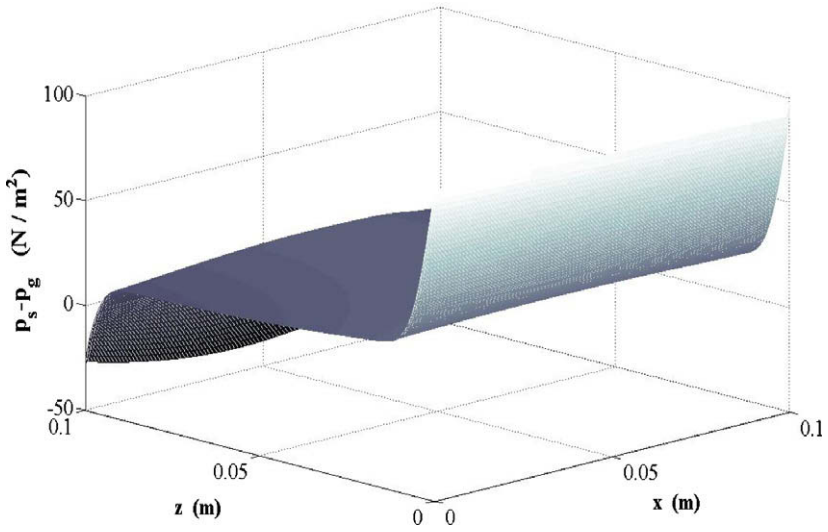

Fig. 2. Pressure difference $\hat{p}, \hat{k}_1 = 0.02$ m^2/s^2, $\hat{k}_2 = 4 \times 10^{-8}$ m^4/s^2.

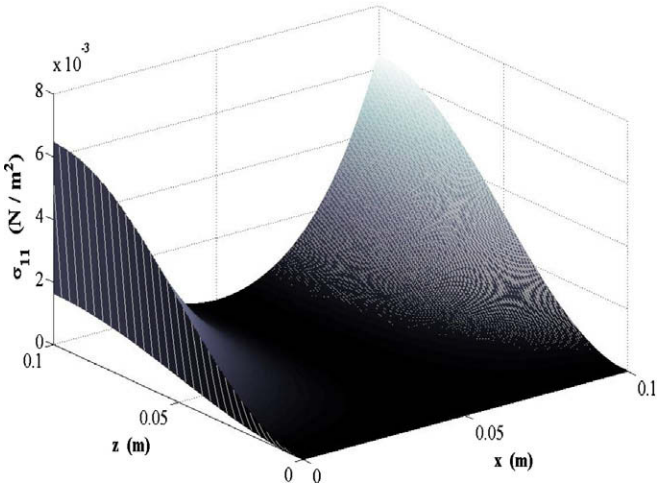

Fig. 3. Residual stress $\hat{\sigma}_{11}, \hat{k}_1 = 0.02\ \mathrm{m}^2/\mathrm{s}^2, \hat{k}_2 = 4 \times 10^{-8}\ \mathrm{m}^4/\mathrm{s}^2$.

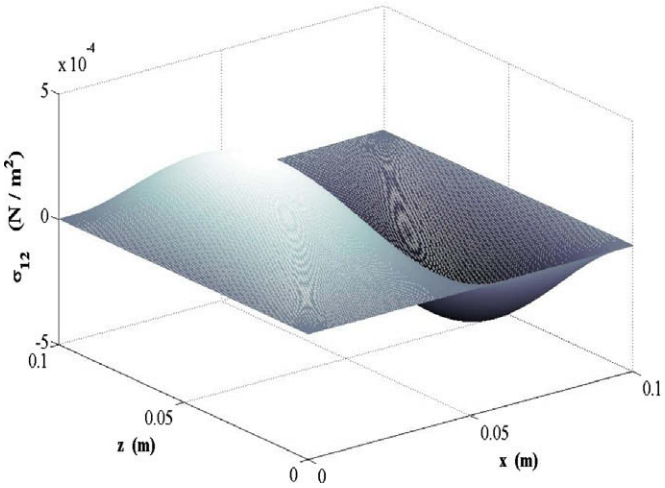

Fig. 4. Residual stress $\hat{\sigma}_{12}, \hat{k}_1 = 0.02\ \mathrm{m}^2/\mathrm{s}^2, \hat{k}_2 = 4 \times 10^{-8}\ \mathrm{m}^4/\mathrm{s}^2$.

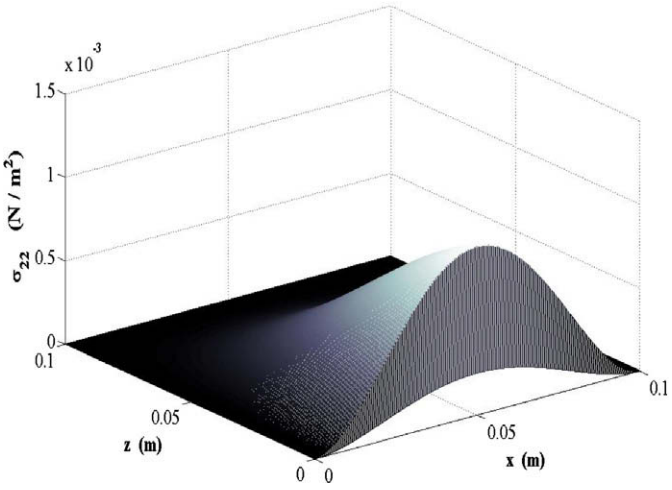

Fig. 5. Residual stress $\hat{\sigma}_{22}, \hat{k}_1 = 0.02\ \mathrm{m}^2/\mathrm{s}^2, \hat{k}_2 = 4 \times 10^{-8}\ \mathrm{m}^4/\mathrm{s}^2$.

Attention should be paid to the choice of the initial conditions for ϕ_s^0 because if the initial profile is too far from a solution of the system, then the numerical method can experience sufficiently long convergence time. For this reason, we proceed to construct an initial condition as follows. First, we note that there exists a maximum value of particle packing. This corresponds to the maximum value of the volume fraction in absence of plastic deformations of the grains, which we denote by ϕ_m. As $\phi_s^0 \to \phi_m$, the solid particles are in such strong contact that the solid phase behaves like a rigid body. For spherical grains, ϕ_m corresponds to the solution of the so-called "minimum packing problem" and is approximately equal to 0.74. Second, the volume fraction has the trend to decrease with $\hat{z}$ due to gravitational forces (beach sand is more dense than water). This trend should be reflected in the initial profile. Further, the initial condition of ϕ_s^0 must be positive everywhere.

Motivated by these criteria, we have used profiles of the form

$$\phi_s^0(\hat{x}, \hat{z}, 0) = 0.74 - F(\hat{z})G(\hat{x}) \tag{75}$$

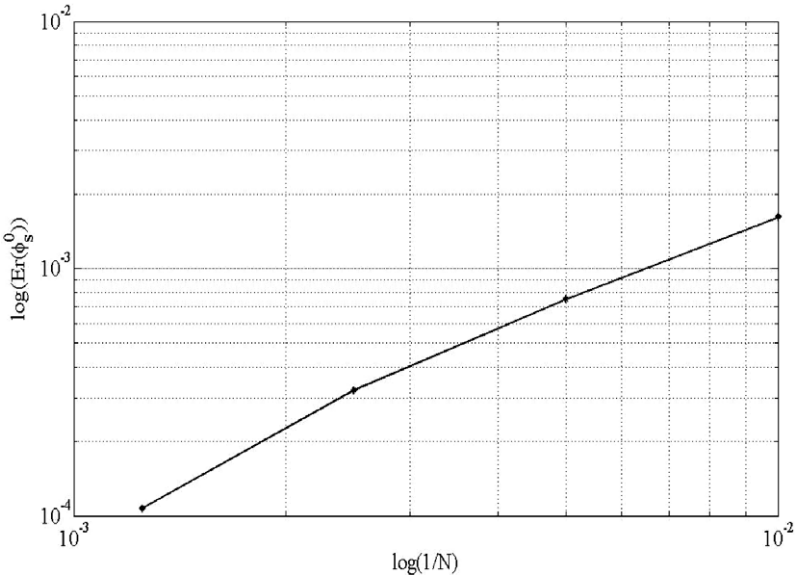

Fig. 6. Grid-convergence study for the solid volume fraction ϕ_s^0.

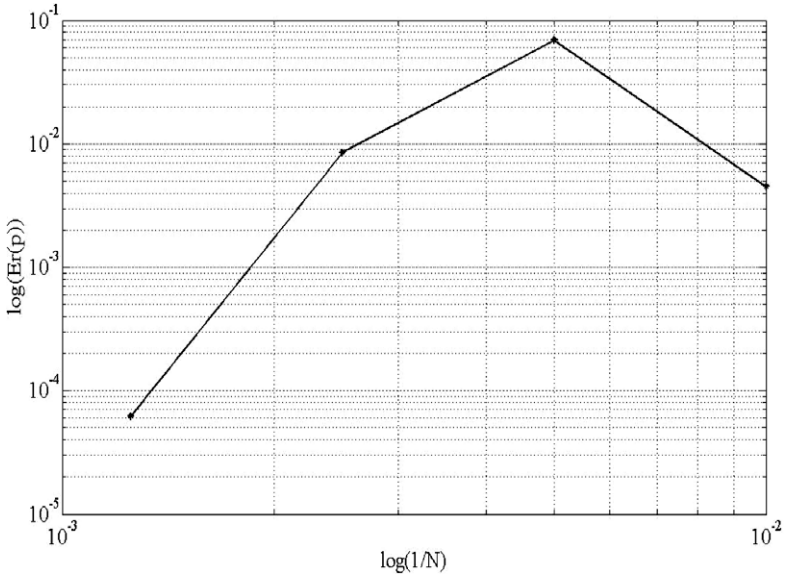

Fig. 7. Grid convergence study for the pressure difference $\hat{p}$.

and perturbations thereof, where $F(\hat{z})$ is a decreasing function in $\hat{z}$. Simple choices for $F(\hat{z})$ and $G(\hat{x})$ are appropriately scaled trigonometric functions or second-order polynomials. In our numerical experiments we have made extensive use of the following profile,

$$\phi_s^0(\hat{x},\hat{z},0) = \left(0.74 - W\hat{x}(L-\hat{x})\sin\left(\frac{\pi\hat{z}}{2L}\right)\right)\left(1 + 0.1\sin\left(\frac{\hat{x}\pi}{L}\right)\right), \tag{76}$$

where W is a constant of order one.

The boundary values are obtained by evaluating the corresponding initial conditions to the boundary points. This implies that the boundary conditions of our problem are of Robin type, since we have Dirichlet boundary conditions for the solid volume fraction ϕ_s^0 and Neumann boundary conditions for the pressure difference $\hat{p}^1$. However, we must caution the reader that imposing boundary values for ϕ_s^0 can be problematic. This is the case with all additional thermodynamic variables, since such variables are generally not controllable on the boundary [15].

6.2. Representative results and numerical convergence

We now present the results from numerical simulations that correspond to a mixture of beach sand and water whose parameter values, initial and boundary conditions follow the set-up formulated above.

Fig. 1 shows the equilibrium distribution of the solid volume fraction, ϕ_s^0; when the initial condition is given by (76). It can be observed that ϕ_s^0 decreases as $\hat{z}$ increases, in agreement with expectations. At the top of the domain ϕ_s^0 has been reduced

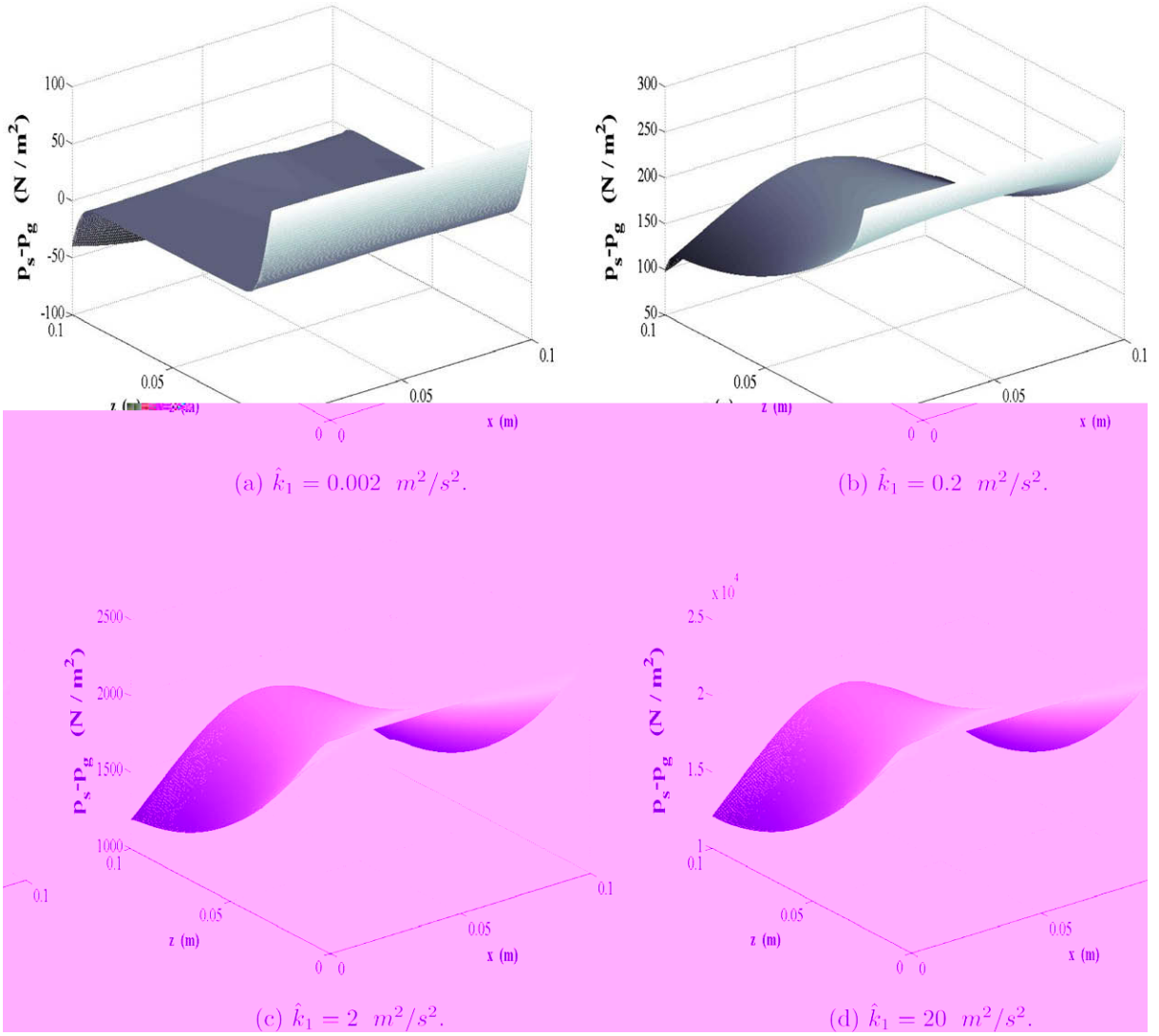

Fig. 8. Pressure difference $\hat{p}, \hat{k}_2 = 4 \times 10^{-8}\ \mathrm{m}^4/\mathrm{s}^2$.

to approximately 60% of its value at ground level. This decrease is mainly due to the density differences between the two phases. Moreover, the convexity of the profile of ϕ_s^0 implies that the concentration of the granular phase is higher in the boundaries than in the interior the domain. It can also be observed in Fig. 1 that the profile of ϕ_s^0 is smooth. This is in agreement with the regularity remarks of Section 2.1 which carry over to the perturbed (39) and (40).

Fig. 2 shows the difference between the solid and gaseous pressures, $\hat{p} = \hat{p}_s - \hat{p}_f$, measured in N/m^2. We observe that $\hat{p}$ is monotonically decreasing with $\hat{z}$, as expected since the right-hand side of (40) is always negative. We also observe the presence of boundary layers in the top and bottom boundaries of the domain. As mentioned above, the role of the residual stresses are non-negligible inside these layers. However, outside these layers the pressure difference $\hat{p}$ is dominated by the gravitational forces. Further, $\hat{p}$ varies little with $\hat{x}$, due to the small value of $\hat{k}_2$.

The maximum value of $\hat{p}$ is equal to, approximately, 100 N/m^2, whereas its minimum value is negative and equal to, approximately, -40 N/m^2. In other words, the overall variation of $\hat{p}$ is at the order of 0.1% of the reference pressure $\hat{p}_0 = 1$ atm. This fact is in accordance with our assumption that the correction terms in the perturbation expansion of Section 2.2 are small, of order ϵ, with respect to the leading order terms.

Figs. 3–5 show the components of the residual stress tensor $\hat{\boldsymbol{\sigma}}$. We observe that the magnitudes of its components are very small: $\|\hat{\sigma}_{11}\| = O(10^{-3})$, $\|\hat{\sigma}_{22}\| = O(10^{-3})$, and $\|\hat{\sigma}_{12}\| = O(10^{-4})$. Therefore, the residual stresses are three to five orders of magnitude smaller than the gravitational forces, in agreement with our estimates above regarding the consequences of the smallness of $\hat{k}_2$. It is interesting to observe that $\hat{\sigma}_{11}$ is the largest component of $\hat{\boldsymbol{\sigma}}$. It increases monotonically with $\hat{z}$ and its maximal values occur at the top left and right corners of the domain. By contrast, the behavior of the other normal stress,

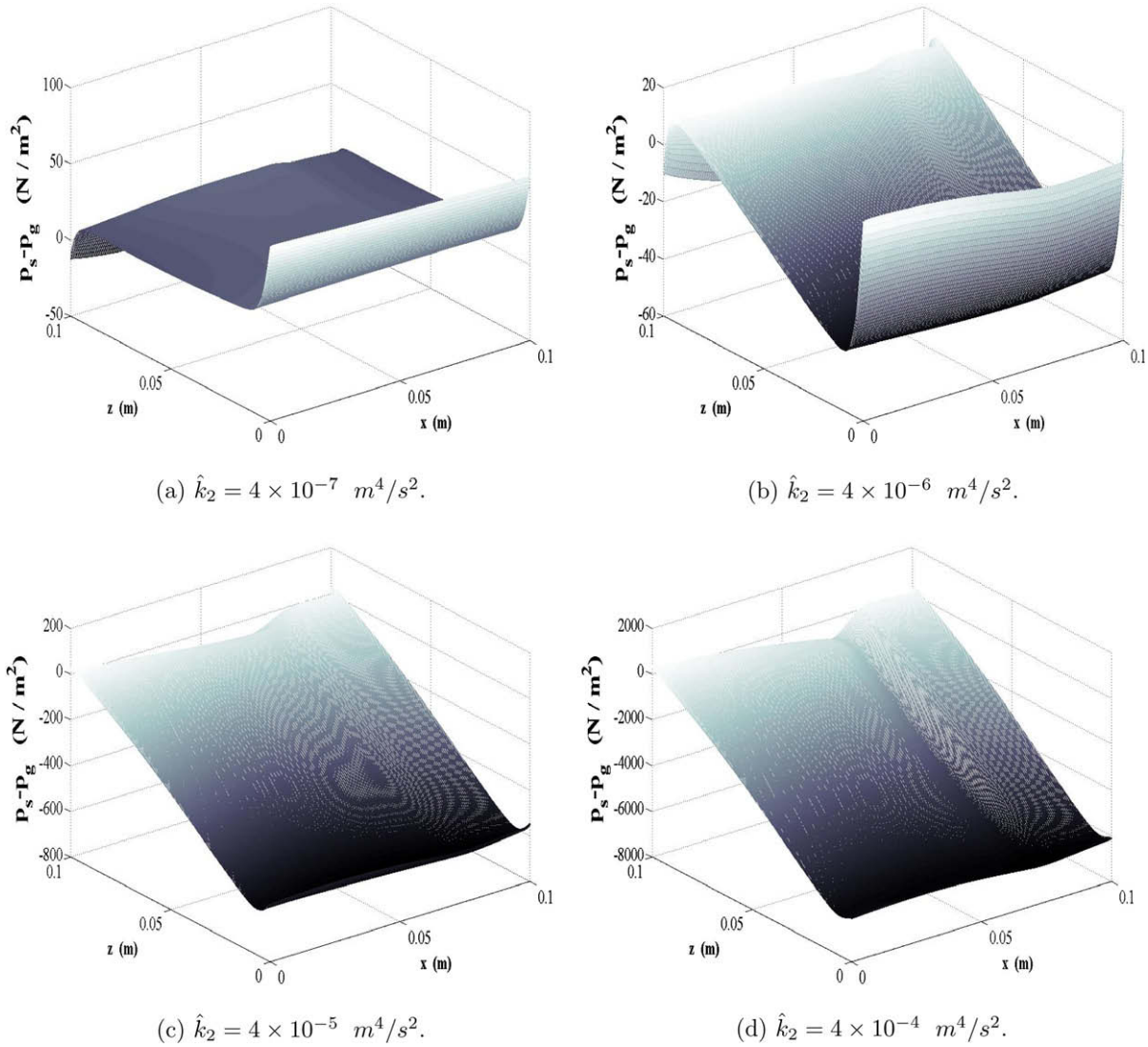

(a) $\hat{k}_2 = 4 \times 10^{-7}\ \ m^4/s^2$.

(b) $\hat{k}_2 = 4 \times 10^{-6}\ \ m^4/s^2$.

(c) $\hat{k}_2 = 4 \times 10^{-5}\ \ m^4/s^2$.

(d) $\hat{k}_2 = 4 \times 10^{-4}\ \ m^4/s^2$.

Fig. 9. Pressure difference $\hat{p}, \hat{k}_1 = 0.02$ m^2/s^2.

$\hat{\sigma}_{22}$ is different: it is decreasing as $\hat{z}$ increases and it takes its maximal value in the middle of the bottom boundary. Finally, the shear stress $\hat{\sigma}_{12} = \hat{\sigma}_{21}$ is the smallest component of the residual stress tensor and has the property that it is anti-symmetric with respect to the axis $\hat{x} = 0.05$ m.

For the case presented here, we have also performed a grid-convergence study. The numerical convergence was tested via the use of the mesh-dependent l^1 norm of the error of the volume fraction ϕ_s^0 and the pressure difference $\hat{p}$, respectively. The mesh-dependent l^1 norm of the numerical error is defined as

$$Er(F) = \frac{1}{N}\sum_{i=1}^{N} |f_i - F_i|, \tag{77}$$

where N is the number of computational cells, F stands for the exact solution, and f stands for the numerical solution. In absence of an analytical solution we used as "exact solution" the numerical result obtained with a very fine grid with 1600×1600 points. The four numerical solutions that have been used for the convergence study correspond to grids of 100×100, 200×200, 400×400 and 800×800 points respectively.

Figs. 6 and 7 show the results of the grid-convergence study for the variables ϕ_s^0 and $\hat{p}$, respectively. It can be directly observed that numerical convergence is achieved with grid-refinement, thus confirming the theoretical results of Section 4.

6.3. Parametric studies

In the course of our numerical experiments we have performed parametric studies with respect to $\hat{k}_1$ and $\hat{k}_2$. These studies are a straightforward way of testing the robustness of the proposed numerical method but they also provide insight on the dependence and sensitivity of the solutions to the values that these parameter take. The results of these parametric studies are summarized below.

First, we fix $\hat{k}_2 = 4 \times 10^{-8}$ m^4/s^2 and let $\hat{k}_1$ vary between 0.002 and 20 m^2/s^2. Changes in $\hat{k}_1$ translate directly into changes of the stiffness of the compaction equation (39) but leave (40) unaffected. Our numerical experiments showed that the changes in the solid volume fraction distribution ϕ_s^0 are very small, at the order of $O(10^{-4})$. Moreover, the variation of $\hat{k}_1$ has virtually no effect on the magnitude and shape of the profile of the residual stresses $\hat{\sigma}_{ij}$.

However, as Fig. 8(a)–(d) shows, the profile of the pressure difference $\hat{p}$ is much more sensitive to change of $\hat{k}_1$. First we observe that the magnitude of $\hat{p}$ increases with $\hat{k}_1$ Further, as $\hat{k}_1$ increases, the gradients of $\hat{p}$ in the top and bottom boundaries are smoothed out, *i.e.*, the boundary layers become thicker. This implies that the residual stresses play a non-negligible role everywhere in the domain. Moreover, as $\hat{k}_1$ increases, the variations of $\hat{p}$ in the $\hat{x}$ direction become larger. This trend can be explained by the fact that as $\hat{k}_1$ increases, the configuration pressure $\hat{\beta}_s$ in the compaction equation eventually becomes dominant over the diffusion term. It is also interesting to note that the monotonic decrease of $\hat{p}$ in the $\hat{z}$ direction is essentially unaffected by variations of $\hat{k}_1$. However, the presence of gradients in the $\hat{x}$ direction results in the appearance of critical points in the interior of the domain.

We also considered values of $\hat{k}_1$ smaller than 0.002 m^2/s^2. Our numerical predictions showed that after a certain threshold, around $\hat{k}_1 = 0.001$ m^2/s^2, there is very little change on the solution profiles. This can be explained by the fact that as the

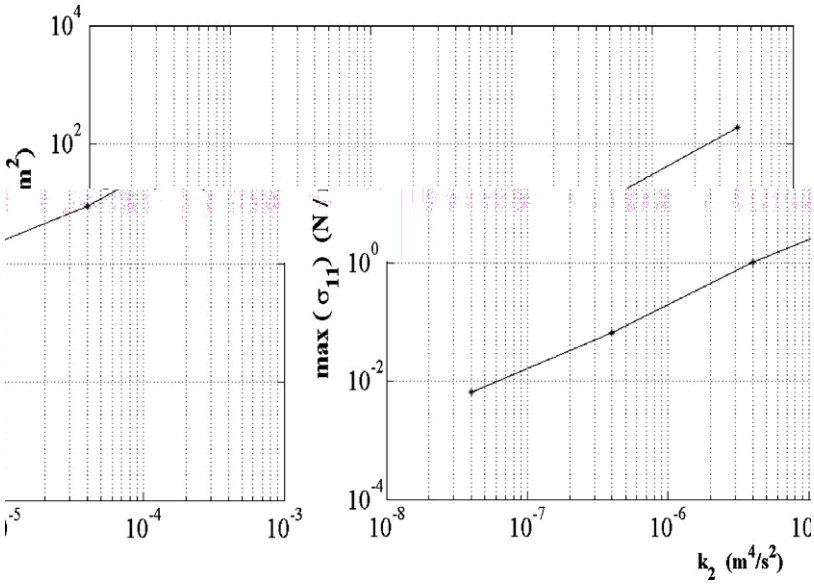

Fig. 10. Max-plot of residual stress $\hat{\sigma}_{11}$.

value of $\hat{k}_1$ gets smaller, so does the configuration pressure $\hat{\beta}_s$ which eventually becomes negligible with respect to the other terms of the compaction equation.

As regards the parametric study for $\hat{k}_2$, we fix $\hat{k}_1 = 0.02\ \mathrm{m}^2/\mathrm{s}^2$ and let $\hat{k}_2$ take values in the range $10^{-8} - 10^{-4}\ \mathrm{m}^4/\mathrm{s}^2$. Similarly to the parametric study for $\hat{k}_1$, we observe very small changes in the profile of the solid volume fraction. In particular, our numerical experiments predict that the changes in ϕ_s^0 with $\hat{k}_2$ are at the order of 10^{-4}.

However, as Fig. 9(a)–(d), 10–12 show, the pressure difference $\hat{p}$ and the residual stresses $\hat{\sigma}_{ij}$ are considerably more sensitive to variations of $\hat{k}_2$. In particular, in Fig. 9(a)–(d) we observe that for values of $\hat{k}_2$ larger than approximately $10^{-6}\ \mathrm{m}^4/\mathrm{s}^2$, the order of magnitude of the pressure difference $\hat{p}$ increases with $\hat{k}_2$. For values of $\hat{k}_2$ smaller than $10^{-6}\ \mathrm{m}^4/\mathrm{s}^2$, the total variation of $\hat{p}$ remains at the order of $100\ \mathrm{N/m}^2$.

Further, we observe that the above value, $\hat{k}_2 \sim 10^{-6}\ \mathrm{m}^4/\mathrm{s}^2$, also acts as a threshold for the behavior of the variation of $\hat{p}$ with $\hat{z}$. Indeed, for values of $\hat{k}_2$ below this threshold, $\hat{p}$ decreases monotonically with $\hat{z}$ because the gravitational forces are larger than the residual stresses $\hat{\sigma}_{ij}$ everywhere in the domain. In contrast, for values of $\hat{k}_2$ above this threshold, the residual

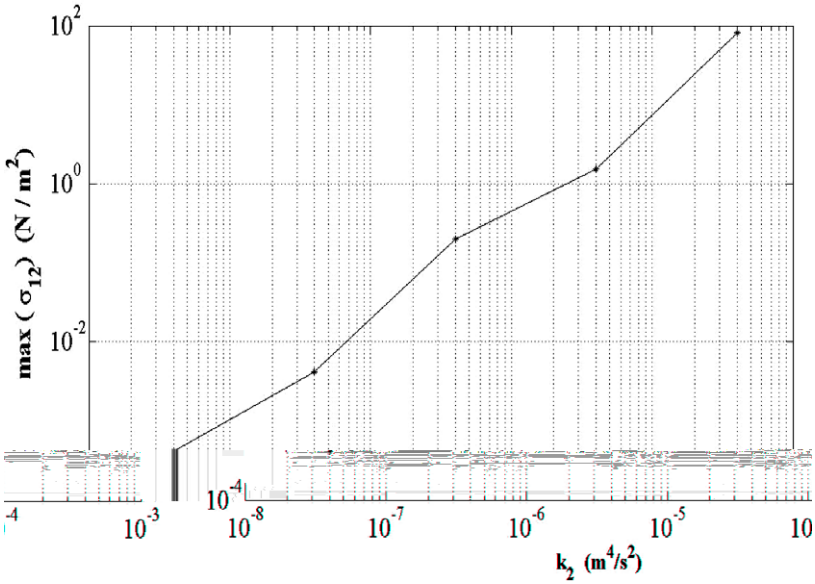

Fig. 11. Max-plot of residual stress $\hat{\sigma}_{12}$.

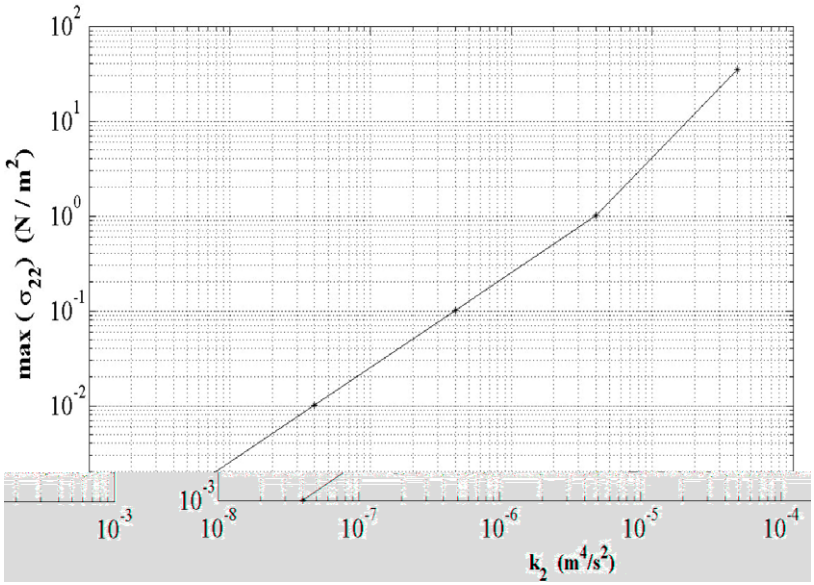

Fig. 12. Max-plot of residual stress $\hat{\sigma}_{22}$.

stresses can balance out the effect of the gravitational forces, thereby changing the monotonicity of $\hat{p}$ along the $\hat{z}$ direction. Also, as $\hat{k}_2$ increases, so does the thickness of the boundary layers. For $\hat{k}_2$ larger than the above threshold, the boundary layers disappear in the sense that the residual stresses $\hat{\sigma}_{ij}$ have non-negligible effect everywhere in the domain.

Also, our parametric study indicates that the shapes of the residual stresses $\hat{\sigma}_{ij}$ are largely unaffected by changes of $\hat{k}_2$. (A similar observation was drawn in the parametric study of $\hat{k}_1$.) Nonetheless, the amplitude of all three residual stresses increase considerably with $\hat{k}_2$, as can be observed in Figs. 10–12. These figures show the variation of the maxima of $\hat{\sigma}_{ij}$ with $\hat{k}_2$. Nonetheless, these residual stresses remain always at least two order of magnitude smaller than the pressure difference $\hat{p}$.

7. Conclusions

In this paper we have presented a theoretical and numerical analysis for the equilibrium limit of the mathematical model for two-phase granular mixture in [13]. At this limit, the model reduces to a coupled, overdetermined system of quasilinear elliptic PDEs. However, at equilibrium, the variations of the phasial densities are expected to be small, which allows a perturbation analysis and, subsequently, decoupling of the system in hand. The perturbed system is supplemented by a compatibility condition which arises naturally and is based on the cohomologies of the gradient operator. Further, we have developed a projection-type, SOR predictor–corrector algorithm for the numerical treatment of the equations based on Ladyzhenskaya's decomposition theorem. As shown herein, the proposed algorithm is both stable and consistent hence, under some standard assumptions, convergent.

We have also conducted a series of numerical experiments by using a water–beach sand mixture as reference. Our numerical studies showed that the residual stresses, which result from non-local effects related to the micro-structure of the mixture, lead to the formation of thin transition or boundary layers. These non-local effects are modelled via the introduction of the volume fraction gradient as an independent thermodynamic variable. The introduction of the volume fraction alone as a thermodynamic variable is not adequate to model such effects which might be important in technological applications. Overall, our numerical experiments indicated that the equilibrium limit of [13] admits solutions that are, intuitively, physically correct. This numerical evidence however, can only serve as a preliminary test of the validity of the model in hand. The crucial validity test is to compare numerical predictions with experimental data.

Our study in the role of the residual stresses and their proper discretization can be useful in the development of numerical methods for two-phase flows of granular mixtures. However, in the case of flowing mixtures, convective effects and residual stresses are expected to give rise to moving interfaces and transition layers. Such structures are known to reduce the regularity of the solutions and the accuracy of standard numerical methods used for their approximation. Therefore, they require the implementation of accurate and robust interface-capturing methods, which is a direction that we intend to pursue next.

As regards other future directions, another natural step forward is the development of an existential theory for the perturbed systems (39) and (40). In fact, existence and regularity results must complement the theoretical and numerical study presented herein for a complete understanding of the equilibrium distributions admitted by the model in hand. To this extent, as mentioned in Section 2.3, the existence analysis of the perturbed system reduces to the study of the third-order vector equation (41). The main difficulty is the overdeterminacy that carries over from the set (39) and (40). This requires the development of a new set of compatibility conditions. However, the fact that Eq. (41) is homogeneous along the x-axis, is expected to simplify the required analysis.

Acknowledgment

The authors gratefully acknowledge the financial support of Fondation Louvain through the Chaire Tractebel – Pôle Energie.

Appendix

The model derived in [13] is based on the assumption that a generalized Gibbs equation holds for each phase,

$$\widehat{T}_i \mathrm{d}\hat{s}_i = \mathrm{d}\hat{e}_i - \frac{\hat{p}_i}{\hat{\rho}_i^2}\mathrm{d}\hat{\rho}_i - \frac{\hat{\beta}_i}{\hat{\rho}_i\phi_i}\mathrm{d}\phi_i - \frac{1}{2\hat{\rho}_i\phi_i}\hat{\Gamma}_i \mathrm{d}(\widehat{\nabla}\phi_i)^2, \quad i = s, f. \tag{78}$$

The balance equations for the fluid phase read

$$\frac{\mathrm{d}\hat{\rho}_f\phi_f}{\mathrm{d}\hat{t}_f} + \hat{\rho}_f\phi_f\widehat{\nabla}\cdot\hat{\mathbf{u}}_f = 0, \tag{79}$$

$$\hat{\rho}_f\phi_f\frac{\mathrm{d}\hat{\mathbf{u}}_f}{\mathrm{d}\hat{t}_f} + \widehat{\nabla}(\hat{p}_f\phi_f) = -\widehat{\nabla}\cdot(\phi_f\widehat{\mathbf{P}}_f^{\nu}) - \hat{p}_f\widehat{\nabla}\phi_s - \hat{\mathbf{f}} - \hat{\rho}_f\phi_f\hat{\mathbf{g}}, \tag{80}$$

$$\hat{\rho}_f\phi_f\frac{\mathrm{d}\hat{e}_f}{\mathrm{d}\hat{t}_f} + \hat{p}_f\phi_f\widehat{\nabla}\cdot\hat{\mathbf{u}}_f = -\phi_f\widehat{\mathbf{P}}_f^{\nu}\odot\widehat{\mathbf{V}}_f^{\nu} - \widehat{\nabla}\cdot\hat{\mathbf{q}}_f + \hat{\mathbf{f}}\cdot(\hat{\mathbf{u}}_f - \hat{\mathbf{u}}_s) - \widehat{E}, \tag{81}$$

whereas the balance equations for the solid phase read

$$\frac{\mathrm{d}\hat{\rho}_s\phi_s}{\mathrm{d}\hat{t}_s} + \hat{\rho}_s\phi_s\widehat{\nabla}\cdot\hat{\mathbf{u}}_s = 0, \tag{82}$$

$$\hat{\rho}_s\phi_s\frac{\mathrm{d}\hat{\mathbf{u}}_s}{\mathrm{d}\hat{t}_s} + \widehat{\nabla}(\hat{p}_s\phi_s) = -\widehat{\nabla}(\hat{p}_s^{v}\phi_s) - \widehat{\nabla}\cdot(\phi_s\widehat{\mathbf{P}}_s^{v}) + \hat{\mathbf{f}} - \hat{\rho}_s\phi_s\hat{\mathbf{g}}, \tag{83}$$

$$\hat{\rho}_s\phi_s\frac{\mathrm{d}\hat{e}_s}{\mathrm{d}\hat{t}_s} + \hat{p}_s\phi_s\widehat{\nabla}\cdot\hat{\mathbf{u}}_s = -\hat{p}_s^{v}\phi_s\widehat{\nabla}\cdot\hat{\mathbf{u}}_s - \phi_s\widehat{\mathbf{P}}_s^{v}\odot\widehat{\mathbf{V}}_s^{v} - \nabla\cdot\hat{\mathbf{q}}_s + \widehat{E}. \tag{84}$$

In the above equations, the operator $\frac{\mathrm{d}}{\mathrm{d}\hat{t}_i} = \frac{\partial}{\partial\hat{t}} + \hat{\mathbf{u}}_i\cdot\widehat{\nabla}$ stands for the material derivative of the ith phase, and $\odot$ stands for the component-wise (Hadamard) product of two tensors.

The quantities $\hat{p}_i^{v}$ and $\widehat{\mathbf{P}}_i^{v}$ result from the natural decomposition of the stress tensor $\mathbf{P}$ to a diagonal part and a traceless deviatoric part

$$\mathbf{P} = -(\hat{p}_i + \hat{p}_i^{v})\mathbf{I} + \widehat{\mathbf{P}}_i^{v}, \tag{85}$$

where $\hat{p}_i$ is the classical (hydrostatic) pure-phase pressure. Also, in single-phase flows, $\hat{p}_i^{v}$ is identified with the bulk viscous pressure. Further, $\hat{\mathbf{q}}_i$ is the heat conduction vector and $\widehat{\mathbf{V}}_i^{v}$ are the traceless deviatoric parts of the deformation tensors $\widehat{\mathbf{V}}_i = \frac{1}{2}(\widehat{\nabla}\hat{\mathbf{u}}_i + (\widehat{\nabla}\hat{\mathbf{u}}_i)^{T})$. Finally, $\hat{\mathbf{f}}$ and $\widehat{E}$ represent the momentum and heat exchanges between the two phases, respectively.

Combining the balance and Gibbs equations for each phase results in an expression for the entropy production rate of the overall mixture. The positivity of the entropy production rate, as required by the second thermodynamic law, is then employed to derive the following constitutive expressions for all terms that describe dissipative processes, including the compaction equation. In the linear regime, these terms can be written as products between thermodynamic fluxes J_i and thermodynamic forces X_k. When off-diagonal terms are ignored *i.e.*, when the couplings between fluxes and forces for $i\neq k$ are set to zero [15], then the final result reads,

$$\widehat{E} = \hat{h}\left(\frac{1}{\widehat{T}_s} - \frac{1}{\widehat{T}_f}\right), \tag{86}$$

$$\hat{p}_f^{v} = \frac{\hat{\Gamma}_f}{3\phi_f}|\widehat{\nabla}\phi_s|^2 - \hat{\zeta}_f\widehat{\nabla}\cdot\hat{\mathbf{u}}_f, \tag{87}$$

$$\hat{p}_s^{v} = \frac{\hat{\Gamma}_s}{3\phi_s}|\widehat{\nabla}\phi_s|^2 - \hat{\zeta}_s\widehat{\nabla}\cdot\hat{\mathbf{u}}_s, \tag{88}$$

$$\hat{\mathbf{q}}_f = \hat{\kappa}_f\phi_f\widehat{\nabla}(\widehat{T}_f^{-1}), \tag{89}$$

$$\hat{\mathbf{q}}_s = \hat{\kappa}_s\phi_s\widehat{\nabla}(\widehat{T}_s^{-1}), \tag{90}$$

$$\hat{\mathbf{f}} = \left(\hat{p}_f - \hat{\beta}_f - \widehat{T}_f\widehat{\nabla}\cdot\left(\frac{\hat{\Gamma}_f}{\widehat{T}_f}\widehat{\nabla}\phi_s\right)\right)\widehat{\nabla}\phi_s + \hat{\delta}(\hat{\mathbf{u}}_f - \hat{\mathbf{u}}_s), \tag{91}$$

$$\hat{\boldsymbol{P}}_f^{v} = \frac{\widehat{\Gamma}_f}{\phi_f}\boldsymbol{\Phi}_s^{v} - \hat{\mu}_f\widehat{\mathbf{V}}_f^{v}, \tag{92}$$

$$\widehat{\boldsymbol{P}}_s^{v} = \frac{\widehat{\Gamma}_s}{\phi_s}\boldsymbol{\Phi}_s^{v} - \hat{\mu}_s\widehat{\mathbf{V}}_s^{v}, \tag{93}$$

where $\boldsymbol{\Phi}_s^{v}$ is defined through the decomposition

$$\nabla\phi_s\otimes\nabla\phi_s = \frac{1}{3}|\nabla\phi_s|^2\mathbf{I} + \boldsymbol{\Phi}_s^{v}, \tag{94}$$

that is, $\boldsymbol{\Phi}_s^{v}$ is a traceless deviatoric tensor. In the above equations, $\hat{\delta}$ and $\hat{h}$ are the coefficients of interphasial momentum and heat transfer, respectively, whereas $\hat{\zeta}_i$, $\hat{\mu}_i$ and $\hat{k}_i$ denote the coefficients of bulk viscosity, shear viscosity and thermal conductivity of the ith phase respectively.

If one assumes, as done in this article, that the fluid phase behaves like a simple Newtonian fluid, then $\hat{\beta}_f = 0$ and $\widehat{\Gamma}_f = 0$.

The model is closed with the compaction equation, which is a rate equation for the solid volume fraction ϕ_s,

$$\frac{\mathrm{d}\phi_s}{\mathrm{d}\hat{t}_s} = \hat{\mu}_c^{-1}\left(\frac{\hat{p}_s - \hat{\beta}_s}{\widehat{T}_s} - \frac{\hat{p}_f - \hat{\beta}_f}{\widehat{T}_f} + \widehat{\nabla}\cdot\left(\left(\frac{\hat{\Gamma}_s}{\widehat{T}_s} + \frac{\hat{\Gamma}_f}{\widehat{T}_f}\right)\widehat{\nabla}\phi_s\right)\right), \tag{95}$$

where $\hat{\mu}_c^{-1}$ stands for the dynamic compaction coefficient.

References

[1] M.A. Goodman, S.C. Cowin, A continuum theory for granular materials, Arch. Rat. Mech. Anal. 44 (4) (1972) 249–266.
[2] S.L. Passman, J.W. Nunziato, P.B. Bailey, Shearing motion of a fluid-saturated granular material, J. Rheol. 30 (1) (1986) 167–192.

[3] M.R. Baer, J.W. Nunziato, A two-phase mixture theory for the deflagration-to-detonation transition (DDT) in reactive granular materials, Int. J. Mult. Flow 12 (6) (1986) 861–889.
[4] J.B. Bdzil, R. Menikoff, S.F. Son, A.K. Kapila, D.S. Stewart, Two-phase modeling of deflagration-to-detonation transition in granular materials: a critical examination of modeling issues, Phys. Fluid 11 (1999) 378–492.
[5] B. Svendsen, K. Hutter, On the thermodynamics of a mixture of isotropic materials with constraints, Int. J. Eng. Sci. 33 (1995) 2021–2054.
[6] Y. Wang, K. Hutter, A constitutive model of multiphase mixtures and its application in shearing flows of saturated solid–fluid mixtures, Gran. Mat. 1 (1999) 163–181.
[7] G. Sciarra, K. Hutter, G.A. Maugin, A variational approach to a microstructured theory of solid–fluid mixtures, Arch. Appl. Mech. 73 (2003) 199–224.
[8] S. Gavrilyuk, R. Saurel, Mathematical and numerical modeling of two-phase compressible flows with micro-inertia, J. Comput. Phys. 175 (1) (2002) 326–360.
[9] H.M. Jaeger, S.R. Nagel, R.P. Behringer, The physics of granular materials, Phys. Today 49 (4) (1996) 32–38.
[10] D.A. Drew, S.L. Passman, Theory of Multicomponent Fluids, Springer, Berlin, 1999.
[11] J. Ding, D. Gidaspow, A bubbling fluidization model using kinetic theory of granular flow, AIChE J. 3 (4) (2004) 523–538.
[12] D. Gidaspow, Multiphase Flow and Fluidization: Continuum and Kinetic Theory Descriptions, Academic Press, 1994.
[13] M.V. Papalexandris, A two-phase model for compressible granular flows based on the theory of irreversible processes, J. Fluid Mech. 517 (2004) 103–112.
[14] S.R. De Groot, P. Mazur, Non-Equilibrium Thermodynamics, Dover, 1984.
[15] D.G. Lebon, D. Jou, J. Casas-Vázquez, Understanding Non-equilibrium Thermodynamics: Foundations, Applications, Frontiers, Springer, Berlin–Heidelberg, 2008.
[16] E.M. Lifshitz, L.D. Landau, Statistical Physics (Course of Theoretical Physics), third ed., vol. 5, Butterworth-Heinemann, 1984.
[17] L.C. Evans, Partial Differential Equations, American Mathematical Society, 2008.
[18] D. Gilbarg, N. Trudinger, Elliptic Partial Differential Equations of Second Order, Springer, Berlin, 1983.
[19] T. Kato, Perturbation Theory for Linear Operators, Springer-Verlag, Berlin, 1966.
[20] P. Dudnikov, S. Samborski, Linear overdetermined systems of partial differential equations, initial-boundary value problems, in: M. Shubin (Ed.), Partial Differential Equations, Encyclopaedia of Mathematical Sciences, vol. VIII, Springer-Verlag, Berlin/Heidelberg, 1996.
[21] Y.G. Sinai, Topics in Ergodic Theory, Princeton University Press, Princeton, NJ, 1993.
[22] D.C. Spencer, Overdetermined systems of linear partial differential equations, Bull. Amer. Math. Soc. 75 (1969) 179–239.
[23] G. Gallavotti, Foundations of Fluid Dynamics, Springer, New York, 2002.
[24] O. Ladyzhenskaya, The Mathematical Theory of Viscous Incompressible Flow, second english ed. revised and enlarged., Gordon and Breach, New York, 1987.
[25] A.S. Kalashnikov, Some problems of the qualitative theory of non-linear degenerate second-order parabolic equations, Russ. Math. Surv. 47 (1987) 169–222.
[26] V.A. Galaktionov, J.L. Vazquez, The problem of blow-up in non-linear parabolic equations, Disc. Cont. Dyn. Syst. 8 (2) (2002) 399–433.
[27] J. Douglas, B.F. Jones, On predictor–corrector methods for nonlinear parabolic differential equations, J. Soc. Ind. Appl. Math. 11 (1) (1963) 195–204.
[28] B. Lessani, M.V. Papalexandris, Time-accurate calculation of variable density flows with strong temperature gradients and combustion, J. Comput. Phys. 212 (1) (2006) 218–246.
[29] A.R. Mitchell, D.F. Griffiths, The Finite Difference Method in Partial Differential Equations, Wiley-Interscience, New York, 1980.
[30] E.E. Rosinger, Stability and convergence for non-linear difference schemes are equivalent, J. Inst. Math. Appl. 26 (1980) 143–149.
[31] H.J. Stetter, Analysis of Discretization Methods for Ordinary Differential Equations, Springer, Berlin, 1973.
[32] G. Baker, P. Graves-Morris, Padé Approximants, second ed., Cambridge University Press, 1996.
[33] S.G. Krein, A.M. Shikhvatov, Linear differential equations on a Lie group, Funct. Anal. Appl. 4 (1) (1970) 46–54.
[34] A.N. Tikhonov, V.Y. Arsenin, Solutions of Ill-Posed Problems, Wiley, New York, 1977.